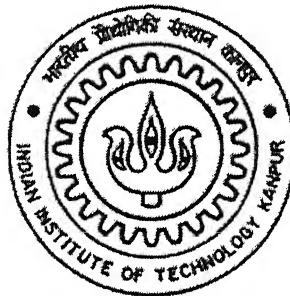# Studies on Propagation Properties of Indoor Optical Wireless Diffuse Channels

A Thesis Submitted

in Partial Fulfillment of the Requirements

for the Degree of

Master of Technology

by

SMITHA K.

to the

Department of Electrical Engineering,
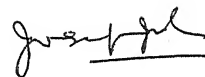
Indian Institute of Technology Kanpur

May, 2005

CERTIFICATE

This is to certify that the work contained in the thesis entitled "**Studies on Propagation Properties of Indoor Optical Wireless Diffuse Channels**", by **Smitha.K**, has been carried out under my supervision and this work has not been submitted elsewhere for a degree.
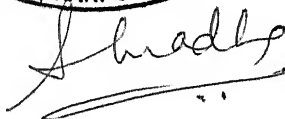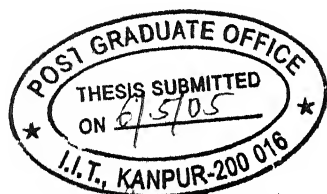
May, 2005

Dr. Joseph John,

Professor,

Department of Electrical Engineering,

Indian Institute of Technology Kanpur

Kanpur – 208 016.

ABSTRACT

Infrared links provide an attractive means to achieve high-speed wireless communications over relatively short distances. As a medium for short-range, indoor communication, infrared offers several significant advantages over radio, including a virtually unlimited spectral region that is unregulated worldwide. This thesis is focused on the study of various characteristic features of indoor infrared diffuse channel. . It is shown that the realistic multipath optical wireless channel can be characterized well by two parameters, viz. the optical path loss and the rms delay spread. The Ceiling bounce model is selected as the basic impulse response model in this work. In the traditional model, the condition to be satisfied is that the transmitter and receiver are co-located. To use this model for the all possible transceiver positions, complex computations are required. This thesis aims at developing a method which can be used to find the impulse response of the system for any transceiver positions with less computational burden. The main parameter of the impulse response (the rms delay spread) is found out using a statistical approach. The pathloss is also calculated separately and both these parameters are used in the modified ceiling bounce model. Detailed studies are done to predict the impact of transmitter and receiver position and their separation from ceiling on rms delay spread, system bandwidth, pathloss and multipath power penalty. The results establish a correlation between path loss and rms delay spread. A study of the dependence of signal to noise ratio and bit error rate on the background noise power and received signal power is also carried out. An experimental set up for the characterization of indoor infrared diffuse channels is proposed. Some of the experiments done using this set up are discussed.

*Dedicated
to*
My Parents

ACKNOWLEDGEMENTS

CONTENTS

LIST OF FIGURES

LIST OF TABLES

LIST OF SYMBOLS

a	Ceiling bounce parameter
a_k	Transmitted symbol
$\hat{a}_k$	Received symbol
A	Average received optical power
A_R	Area of receiving element
$Ab(t)$	Impulse response of transmitter filter
BER	Bit error rate
BER_0	Bit error rate at zero intersymbol interference (ISI)
c	Velocity of light
f_{3dB}	3 dB cut off frequency of the system
FOV	Field of view of receiver
$F_T(t)$	Complex electric field of signal
$g(t)$	Impulse response of receiver filter
G_0	Optical channel dc gain
$h(t)$	Impulse response of the infrared channel
$h_c(t)$	Ceiling bounce model for multipath dispersion
$h^{(k)}(t;S,R)$	Impulse response after k reflections of light
h_0	zero-sample
h_1	Separation of transmitter from the ceiling
h_2	Separation of receiver from the ceiling
h_k	discrete time impulse response at time $=kT$
H	height of ceiling

$H(f)$	Frequency response of the infrared channel
Δh	Height of irregularity
I_2	Noise bandwidth factor
$I_T(t)$	Intensity of transmitted signal
M	Length of impulse response tail
n	Mode number of radiation pattern
$n(t)$	Gaussian white noise
$\hat{n}$	Normal to the surface
n_k	received noise power at time $=kT$
P_n	Background noise power
P_r	Received signal power
P_s	Incident signal power
P_t	Transmitted signal power
PL	Path loss
q	Charge of electron
$Q(x)$	Gaussian Q function
R	Responsivity of photodiode
R_b	Transmitted bit rate
SNR	Signal to noise ratio of the system
t	Time
T	Bit duration
$u(t)$	Heaviside's unit function
x_1	X position co-ordinate of the transmitter
x_2	X position co-ordinate of the receive
$X(t)$	Message signal
X_k	Intersymbol interference (ISI)
y_1	Y position co-ordinate of the transmitter

y_2	Y position co-ordinate of the receiver
y_k	received signal at time $=kT$ (k^{th} received sample)
$Y_R(t)$	Intensity of received signal
α_k	Attenuation factor
χ	$A/2\sigma$
χ_0	χ at zero intersymbol interference (ISI)
δ_k	Unit impulse function at time $=kT$
ϕ	Observation angle
λ	wavelength of light
μ	Mean delay
θ_i	Incidence angle of light at a surface
ρ	Reflection coefficient
σ^2	Noise variance
σ^2_{shot}	Shot noise variance
$\sigma^2_{thermal}$	Thermal noise variance
σ^2_{total}	Total noise variance
τ_{rms}	RMS delay spread

CHAPTER 1

INTRODUCTION

The emergence of portable computing devices such as laptops, palmtops and personal digital assistants has fuelled the demand for mobile connectivity and hence, led to the development of wireless local area networks (LANs). Wireless communications have always offered an alternative solution to the fixed network, which introduce difficulties in construction and rewiring during the initial system set up and later during the expansion phases. The benefits of an alternative flexible network are many in terms of its mobility and portability. Trends in communication suggest that the future network may consist of a fiber-optic network and wideband wireless short-range access over a wireless channel. Portable terminals should have access to all of the services that are available on high-speed networks. Unlike their wired counterparts, portable devices are subject to severe limitations on power consumption, size and weight. The desire for inexpensive, high-speed links satisfying these requirements has motivated the recent interest in infrared wireless communication.

Traditionally, radio frequency transmission was used in wireless applications. However, the RF spectrum is so congested that it is very difficult to accommodate high bit rate applications. The optical systems with low implementation complexity and no spectrum license requirements provide a possible solution. The optical infrared energy can typically confine within the communication environment. This eliminates the problems of interference generated by neighboring users and offers a degree of security at the physical level. The same transmission equipment and optical wavelength can be reused in other parts of the building. Optical wireless systems also offer immunity from signal fading, which is a major problem in RF communication systems. As such, indoor infrared communications has recently gained importance, especially in view of the increased data mobility requirements of users for both computing and communications.

Infrared communications were mainly studied during the 1960's as an alternative for mobile radio communications. But, no real system for indoor coverage using infrared links was seriously considered. Recently, infrared has gained ground with operators seeking to cover areas that require high bit rate services such as the office areas. Serious work on indoor optical wireless systems started during early 90's. At present it is a very rapidly developing research area and there is huge interest and commitment in this area by the major communication industries due to its enormous commercial applications.

In order to correctly and efficiently deploy a communication system, the system designer must have a sound knowledge of the channel. This can be done through experimentation and modeling with methods that are accurate enough to account for all significant channel characteristics.

This thesis deals mainly with the study of different characteristic features of indoor optical wireless channels. Simulation studies are done on the various propagation properties of the optical signal. The main objectives of the work are discussed in the following section.

1.1 THESIS OBJECTIVES

The objective of the thesis is to completely characterize the indoor optical wireless channel by studying all the important factors governing signal propagation. A widely accepted channel model is considered as the basis for simulation. The parameter which defines the model is found using a different approach and extensive studies are done. The objectives are summarized as follows:

- To find the RMS delay spread of the transmitted optical signal due to multi path propagation.
- To study the effect of transmitter and receiver location and room dimensions on RMS delay spread.

- To find the path loss of the infrared channel

- To find the impulse response, frequency response and estimate the system bandwidth.

- To find the power penalty due to multipath propagation

- To obtain the correlation between RMS delay spread and pathloss of the channel

- To set up an automated experimental system to measure the infrared channel properties.

1.2   THESIS ORGANISATION

Chapter 2 gives a review of the indoor optical wireless systems. The basic components of the optical wireless systems and link configurations are discussed. Comparison of infrared systems with its RF counter part is also discussed. A brief literature survey of the infrared channel modeling and characterization is also presented. Chapter 3 summarizes the theoretical background for the indoor channel characterization. Our modified ceiling bounce method to find the impulse response of indoor channel is discussed in details. Chapter 4 deals with the simulation studies of indoor channel. The results are also discussed. Chapter 5 explains the experimental characterization. It gives a description of experimental set up and experiments conducted. The results of the experiment are discussed in brief. Finally, chapter 6 presents the conclusions of the work and future improvements that may be possible in the channel studies.

CHAPTER 2

REVIEW OF INDOOR INFRARED WIRELESS SYSTEMS

2.1 INTRODUCTION

The wireless systems widely used today utilizes radio waves, but this alone may not be sufficient for the future. Modern digital communication systems require high data rate capabilities. However, the radio spectrum is regulated and saturated. An alternative medium is infrared communications, which appear to be a very attractive way to complement radio.

Infrared communications have found many areas of use. Almost every home includes a television set which is controlled by an infrared remote control. Also, there is a standard for communications between two computers using infrared. This standard is called IrDA (Infrared Data Association), and has been included in almost every portable computer or even mobile phone. This supports speeds up to 115Kb/s but the limiting factor is that the distance between the two terminals has to be low, and a line of sight is always needed. Infrared communications are very successful in the field of directed communication between two buildings. Although very high rates up to hundreds of Mb/s can be achieved, it has the disadvantage of being unsustainable in heavy weather conditions such as snowfall or fog. The link cannot be sustained then, due to the increased path loss between the terminals.

This chapter provides a small review of the indoor infrared wireless communication system. It explains the basic components, link configurations, a comparison with radio, and a literature survey of the important works in this field. Finally, some of the practical systems reported are discussed.

2.2 BASIC OPTICAL WIRELESS SYSTEM

The basic sub systems of an optical wireless system are Transmitter (LEDs or Laser diode based), the Channel (the medium between the transmitter and the receiver) and the Receiver (PIN or APD based). The link length can vary from a few meters to a few km. The block diagram of a typical optical wireless communication link is shown in fig. 2.1
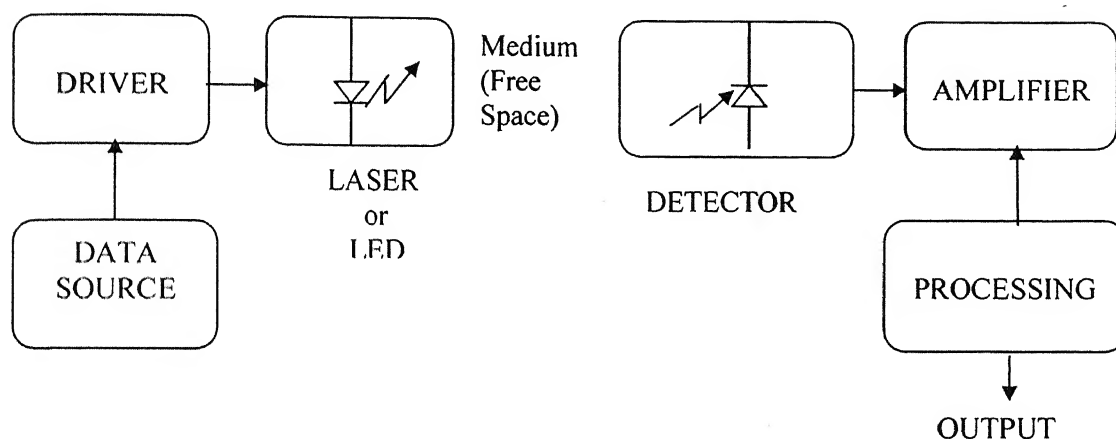
Fig. 2.1 **Block Diagram of an Optical Wireless Communication Link**

The electrical information signal produced by the source modulates an optical carrier. This is commonly called Intensity modulation (IM). The modulated optical carrier is propagated as a light through the channel. At the receiver this field is optically collected and converted back to an electrical signal by a detector, which is further processed by electronic stages to recover the original information with an acceptable level of error.

2.2.1 Transmitter

The transmitter side consists of the data source, driver circuits and the light source. There are two basic light sources, the laser diode (LD) and the light emitting diode (LED). Since eye safety is a major consideration for indoor applications, the optical source need to be chosen carefully. LEDs are the preferred choice for indoor

use. Since the light intensity of an LED may not be sufficient for most applications, LED arrays may have to be used. Another popular solution is to use a laser diode with a diffuser. A comparison between the characteristics of LEDs and LDs are given in Table 2.1.

Characteristics	Light Emitting Diodes	Laser Diodes
Spectral Width	25-100 nm	$<10^{-5}$ to 5 nm
Modulation Bandwidth	Tens of KHz to tens of MHz	Tens of MHz to tens of GHz
E/O Conversion Efficiency	10 to 20%	30 to 70%
Eye Safety	Generally considered eye-safe	Must be rendered eye-safe. Especially for $\lambda<1400$nm.
Cost	Low	Moderate to high

Table 2.1 Comparison between LEDs and LDs [1]

2.2.2 Free Space Medium

The link budget for a free space link are strongly determined by the atmospheric loss along the propagation path, which comprises of free space loss, clear air absorption, scattering, refraction, and scintillation. All forms of optical wireless systems experience free space loss. Other sources of atmospheric loss are applicable to long distance systems only. Free space loss defines the proportion of optical power arriving at the receiver that is usefully captured within the receiver's aperture.

2.2.3 Receiver

The function of the receiver is to convert the optical signal back to the original electrical signal. Receiver consists of a PIN or APD photodetector, preamplifier, post amplifier and a comparator to obtain digital data. PIN and APD operate in reverse bias, also known as photoconductive mode of operation. The advantages of photoconductive operation are higher speed, lower capacitance, and better linearity.

The photodetector and amplifier are sources of noise at the receiver side. The noise in a photodiode can be of two types; the first one called the shot noise due to dark current, and the second one called the thermal noise of the shunt resistance, also known as Johnson noise. The important requirements on the photodiodes for wireless communications are high quantum efficiency, fast response time, low capacitance, low dark current and low avalanche excess noise. It is desirable to use a large area photodetector since shot noise limited SNR is proportional to the detector area. However large area detectors have high capacitance, which can limit receiver bandwidth and greatly increase receiver thermal noise. It is desirable to reduce the required detector physical area by the use of an optical concentrator, which accepts light from a large collection area and concentrates it to the somewhat smaller detector area.

2.3 COMPARISON WITH RADIO

Infrared communications offer advantages and some disadvantages when compared with the analogous radio links. . Table 2.2 gives a comparison between the two systems

Property	Radio	Infrared
Path Loss	High	High
Multipath Fading	Yes	No
Multipath Dispersion	Yes	Yes
Bandwidth Limitation	Regulatory	Photodiode
Dominant Noise	Interference	Background Noise
Signal Transmitted	Amplitude	Power
Wall Penetration	Yes	No

Table 2.2   Comparison between Infrared and Radio Channels [2]

As seen from the comparison, infrared shares some properties with radio, although there are some significant differences. These are discussed in detail below.

1.   Multipath fading is not present in infrared channels since the area of the receiving photodiode spans several thousands of wavelengths. The output current of the photodiode will be proportional to the integral of the squared electric field over the entire area of the photodiode surface. Thus a single photodetector can provide a significant spatial diversity, which will prevent multipath fading. Multipath dispersion is present in infrared channels also. If a short pulse is sent through the channel, the pulse broadens due to dispersion and Inter symbol interference occurs. The dispersion is the result of the reflective properties of the channel, which transforms a narrow pulse to a wider version. This limits the data rate and increases the bit error rate.

2.   In radio, the main limitation of bandwidth is due to regulation, since the bandwidth has to be licensed before being used. On the other hand, in infrared the limitation is posed by the channel and the various devices.

3.   The dominant noise in cellular radio communications is interference from adjacent cells. In infrared systems, noise comes from the background. The three main sources of ambient light are sunlight, incandescent lamps and fluorescent lamps [3], [4], [5]. Infrared links cannot sustain operation in direct sunlight, unless special filters or very directional sources and receivers are used. Artificial sources of ambient light produce a periodic interference signal in infrared wireless receivers which, if ignored, has the potential to degrade link performance. These lights have a wide spectrum and they also emit higher power infrared radiation during warm up thus degrading infrared communication.

4.   Although the infrared channel is related to the linear gaussian channel, there is a difference between the two. The input of infrared channel represents power and not amplitude unlike radio. This gives rise to two constraints; first, the signal

must be positive and second, its average value must not exceed a prescribed value [6] for safety reasons.

The transmitted power in the infrared domain is described by

$$\lim_{T \to \infty} \frac{1}{2T} \int_{-T}^{T} x(t)dt \leq P$$

where

x (t) is the instantaneous value of the transmitter signal (Watts)

P is the maximum value of the power allowed to be transmitted due to safety reasons

T is the duration of communication (sec)

5. Infrared radiation does not penetrate opaque objects, and walls efficiently separate two cells. Security is high since the radiation is confined within the cell. On the other hand, less coverage can be achieved with an infrared link, and base stations have to be placed within every room of operation.

The following points summarise the advantages and drawbacks of infrared communications over radio.

- Infrared offers unregulated bandwidth: 200 THz in the 700-1500 nm range.

- There is no interference from adjacent cells and security is high.

- No Multipath fading.

- Higher capacity per unit volume.

- Cost effective at rates above 100 Mb/s.

The drawbacks are:

- Multipath dispersion is present.

- Large amounts of radiation can be harmful to humans.

- Strong interference from daylight, light sources, remote controls and other devices.

2.4   LINK CONFIGURATION

Indoor optical wireless can employ various designs, and it is convenient to classify them according to two criteria. This classification scheme is shown in fig. 2.2 [1]

	Directed	Hybrid	Non-Directed (Diffuse)
LOS			
Non LOS			
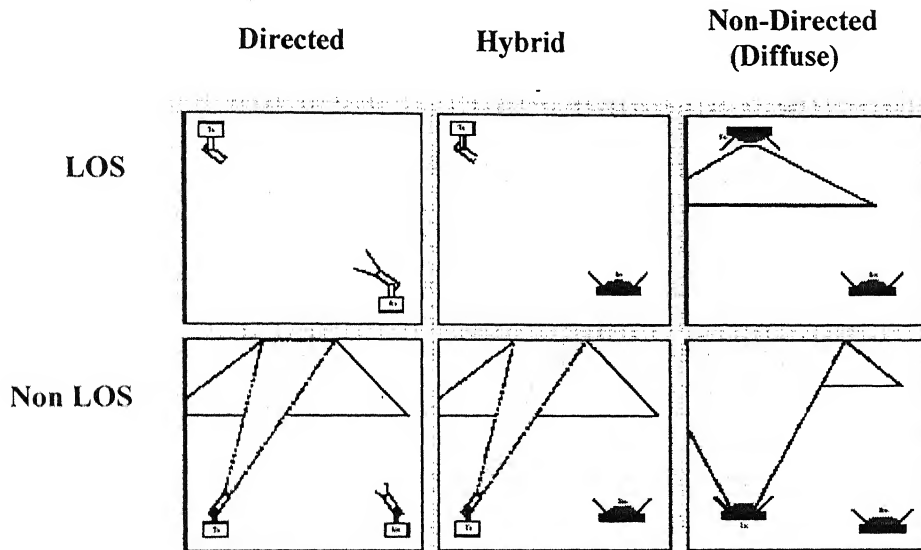
Fig. 2.2   Classification Of Infrared Links[1]

The first criterion is the directionality of the transmitter and receiver. Directed links employ directional transmitters and receivers, which must be aimed in order to establish a link. Nondirected links employ wide-angle transmitters and receivers, alleviating the need for pointing. Directed link design maximizes power efficiency, since it minimises path loss and reception of ambient noise. On the other hand, nondirected links may be more convenient to use, particularly for mobile terminals, since they do not require aiming to the transmitter or receiver. It is also possible to establish hybrid links, which combine transmitters and receivers having different degrees of directionality.

The second classification criterion relates to whether the link relies upon the existence of an uninterrupted line-of-sight (LOS) path between the transmitter and receiver. LOS links rely upon such a path, while non-LOS relies upon reflection of the

light from the ceiling or some other diffusely reflecting surface. LOS link design maximises power efficiency and minimises multipath distortion. Non-LOS link design increases link robustness and ease of use, allowing the link to operate even when barriers are there between the transmitter and receiver. The greatest robustness and ease of use is achieved by the nondirected-non-LOS link design which is often referred to as diffuse link.

2.4.1 Line of Sight Systems

Line of Sight systems employ high degree of directionality of the transmitter and receiver and uninterrupted LOS. LOS link design maximises power efficiency and minimises multipath distortion. The performance of the link relies up on the existence of an uninterrupted LOS path between the transmitter and receiver. The main drawback is the lack of mobility and susceptibility to blocking. The optical sources must be Class 1 eye safe; hence LEDs have to be used in place of LDs which limits the capacity to a few megabits per second

These types of links are used for applications in which the terminals are relatively fixed, such as desktops computers in an office. One of the most widely adopted standards is the Infrared Data Association standard (IrDA).

2.4.2 Diffuse Systems

The greatest robustness and ease of use is achieved by the non-directed, non-LOS design, which is often referred to as diffuse link. However, diffuse systems have a higher path loss than their LOS counterparts, requiring higher transmitter power and a receiver having large light collection area.

This type of topology overcomes the blocking problem by relying on the high reflectivity of common building materials, so that a significant fraction of the received signal arrives at the receiver from a number of angles. Such a topology is extremely

flexible and can be used in either organised or ad-hoc networks. However the bit rate that can be achieved is very less compared to the LOS systems. In addition, optical losses associated with the link are much greater than LOS systems.

In case of an entirely diffuse link, the optical power launched into a closed room is scattered by the walls, ceiling, floor and furniture. After some reflections, the irradiance is almost uniform, so that the detector does not need to be oriented toward the emitter. Full mobility within the room is allowed and there are no shadowing effects caused by moving persons or machines. There are two limitations for diffuse links: the emitted optical power has to be large enough to cover the whole volume, and multipath dispersion limits the data rate. Multipath propagation causes a spread of the transmitted pulse, which may result in a loss of pulse amplitude and inter symbol interference. Hence, there is a maximum transmission speed which depends on the room size and the reflection coefficients inside the room.

2.5   LITERATURE REVIEW

Detailed characterisation of the infrared wireless channel is essential for effective communication link design. In the last two decades, considerable amount of research have been carried out in infrared wireless communication field. A literature search shows that both experimental and numerical investigations have been carried out in the areas related to infrared channel modeling and characterization.

2.5.1 Simulation Methods

Gfeller and Bapst [7] **(1979)** are considered as the pioneers in infrared communications, who studied the channel characteristics in the 70's. Their work suggested the use of IR channel for indoor communications. They studied various channel parameters, such as the reflection properties of many materials. They were also the first to suggest that the reflections from surfaces can be modelled as Lambertian. In

this paper, a method for calculating power for a given geometry of the channel is presented, although no specific algorithm is described. A study on link properties and infrared receivers is also presented. Finally, an experimental system is proposed, which offers data rates up to 64 kbps.

Barry *et.al.*, in their paper [1],[8],[9] (1993), discretised the room into small facets and calculations were done to find the impulse response of the channel for as many reflections as required. This is a recursive method. In order to find the response due to the kth reflection, one had to know information about the $(k-1)^{th}$ reflection and also the LOS response. This method is very attractive, but has the disadvantage of having very long simulation times and very demanding requirements on the processing power. This technique has been widely used in academia and industry, and is the standard model for calculating the impulse response of indoor channel, although the memory requirements and durations are quite high in order to produce accurate results.

In [10] (1997), a different approach was taken by Carruthers and Kahn who developed the Ceiling bounce model based on the claim that realistic multipath infrared channels can be characterised by just two parameters, viz. the optical path loss and root mean square(RMS) delay spread. Firstly, an exponential decaying model is presented for the impulse response. Later in this paper, a ceiling bounce model is presented, which adopts a two stage modelling approach - first assuming an infinitely large room, i.e. considering only a single reflection from the ceiling, and then making a correction which takes into account the position of the transmitter and receiver within the room. This model does not account for presence of obstructions and multiple reflections. However, this method presents a way to characterise the infrared channel completely in terms of the multipath power penalty and delay spread.

Perez Jimenez [11], [12] (1997) suggested a statistical model based on several experiments that calculates the impulse response of the channel. They come up with a

closed-form expression for the RMS delay spread. Hence this is a fast approach to modelling the indoor IR channel. However, this method is not used by most researchers. It is likely that the simulation results are not very accurate under all conditions.

Hernandez *et.al.* [13](1998) also developed a computationally efficient algorithm based on Monte Carlo analysis to arrive at the impulse response of the indoor channel.

Carruthers *et.al.* [14](2002) developed an iterative site based method for estimating the impulse response of wireless infrared channels. This method can include any number of multiple reflections and can account for all types of obstructions and shadowing effects. This is computationally more effective than the recursive method used by Barry *et. al.* [8],[9].

2.5.2 Experimental Studies

Experimental measurements of indoor infrared channel were performed at the **University of Ottawa** [15], [16] **(1994)** over a 40MHz band. This paper presents the results of a frequency response measurement at eight different sites in a university building. The experimental results prove that the indoor infrared wireless channel is quite dynamic, with great variations in the channel characteristics for data collected in different rooms, in different locations within the same room, and for different orientations of the receiver at the same location for the same room.

Later, **Krause** *et.al.* [17] **(1995)** did an experimental characterisation of infrared channel over 2-300 MHz range by using swept-modulation frequency technique. From these data, they calculated the impulse response, RMS delay spread and path loss of more than 100 different channel configurations. They characterised 'shadowed' and 'non-shadowed' line of sight as well as diffuse channels in this work.

Pakravan *et.al.* [18], [19] **(2001)** extended the work at the University of Ottawa up to a band of 400 MHz for different configurations. They mainly studied the effect of receiver rotation and shadowing on the properties of indoor infrared channels. Using statistical techniques, methods are presented to predict the path loss variations for small changes in the receiver direction. The demonstrated results give a correlation between the channel path loss and RMS delay spread for both LOS and diffuse configurations.

All these experiments have results in good agreement with the simulation results obtained in earlier works, thus validating the different channel impulse response models.

The models presented in Sec.2.5.1 are some of the important ones presented so far in the infrared modelling world. Although the detail and accuracy of the model presented by Barry *et.al.*[8],[9] may be high, its requirements are far too costly for a very detailed simulation. Other techniques are not that accurate, but have less computational burden.

2.6 PRACTICAL SYSTEMS REPORTED FOR INDOOR APPLICATIONS

This section presents different practical systems reported in wireless infrared communication field.

Gfeller *et.al.* of IBM **(1978)** [7] were the first to propose the use of infrared for a wireless LAN. In this system, the transmitter emits infrared energy into a broad optical beam, and the receiver has a wide field of view. The base station illuminates the ceiling with a broad optical beam of 800mW, so that the ceiling acts as a distributed secondary source. The bit rate used was 125 kb/s and the range was 10-20m depending on the severity of the ambient light noise.

Yun and **Crawford** proposed the first Line of Sight (LOS) infrared wireless network **(1985)** [9]. It uses 1Mb/s directed LOS links to connect multiple terminals to a

centrally located base station. The base station transmits 165 mW into a circularly symmetric planar beam with a 3° vertical beam width, while the terminals transmit 5 mW into a narrow 2° beam. The range was 50m. To provide full duplex transmission, different wavelengths were used for the uplink and the downlink.

Chu and **Gans** (**1987**) [9] have reported another LOS system in which the base station has a number of discrete 1° pencil beams carrying 1mW of power each. They were able to achieve a data rate of 50 Mb/s at a range of 30m.

A product launched in the market by **BICC** Communications (**1992**) [9] used directed LOS configuration. It is reported to have a throughput of 4 Mb/s and a range of 24m. **JOLT** Ltd. (**1993**) [9] announced a 125 Mb/s LOS system with a range of 30m when directionality was 1° transmitter beam and a 6° receiver FOV. The range was only 1m for this system when the directionality was low, i.e. 55° transmitter beam and a 55° FOV.

Kahn *et.al.* reported (**1997**) [1] an experimental 50 Mb/s diffuse infrared link using OOK. The transmitter uses a cluster of eight LDs whose output is passed through a diffuser. The output is Lambertian with an average power 475 mW at a wavelength 806 nm. The receiver has a large collection area, wide FOV and narrow pass band.

Table 2.3 summarises the details of many of the infrared systems reported so far. It consists of both diffuse and LOS systems.

Year	Type	Data Rate (Mb/s)	Range (m)
1978- Gfeller	Non-directed, Non- LOS	0.125	20
1985- C S Yun *et al*	1st LOS	1	50
1987- T S Chu *et al*	LOS	50	30
1992- B Berline	LOS	4	24
1993- JOLT Ltd.	LOS	125	30
1995- J R Barry *et al*	Non-direct LOS	100	4
1997- J M Kahn *et al*	Diffused	50	10x10
1999- D J Heatley, *et al*	LOS	1000	--------

Table 2.3   **Practical systems reported for indoor applications [5]**

CHAPTER 3

INFRARED CHANNEL MODELLING AND CHARACTERISATION

This chapter describes the tools used to model the infrared channel. The channel under study is the infrared diffuse channel, in which there is no need for Line-of-sight between the transmitter and receiver, and communication may rely on scattered radiation from the walls of the room. In this way, mobility is increased, and shadowing does not have a large impact on the link.

3.1 INTENSITY MODULATED/ DIRECT DETECTION CHANNELS

Modulation techniques for the radio wireless systems include amplitude, phase and frequency modulation as well as some generalisations of these techniques. Radio receivers usually use heterodyne or homodyne detection techniques which requires a local oscillator and mixer. Efficient operation of mixer relies upon the fact that it receives both the carrier and the local oscillator output in a common electromagnetic mode [1].

In a low cost wireless infrared system, it is extremely difficult to collect appreciable power in a single electromagnetic mode. This spatially incoherent reception makes it difficult to construct an efficient heterodyne or homodyne converter for AM, PM, or FM. For infrared links, the most viable modulation is the intensity modulation (IM), in which the desired waveform is modulated onto the instantaneous power of the carrier. Intensity modulation is performed by varying the current of a laser diode or an LED. The most practical down-conversion technique is direct detection (DD), in which a photodetector produces a current proportional to the received instantaneous power, i.e., proportional to the square of the electrical field [1].

3.1.1 Channel's Baseband Model [15]

For an IR wireless transceiver that operates on the intensity modulation-direct detection principle, the propagation medium can be replaced with an equivalent baseband channel model. Let $X(t)$ denote the normalised message signal($-1 < X(t) < 1$). The positive signal $A[1 + \mu X(t)]$, modulates the intensity of light source, where μ is a positive constant, $0 < \mu < 1$. The intensity of the transmitted signal is then given by

$$I_T(t) = |f_T(t)|^2 = A[1 + \mu X(t)] \tag{3.1}$$

$f_T(t)$ being the complex field of the transmitted signal. Denoting the complex field of the signal received through the kth reflection at a given point on the photodetector surface by $f_k(t)$, $k = 0,1,2,\ldots,N$

$$f_k(t) = \sqrt{\alpha_k} \sqrt{A[1 + \mu X(t - t_k)]} e^{-j\omega_0(t - t_k)} \tag{3.2}$$

where $\omega_0 = 2\pi f_0$, f_0 being the frequency of light. The attenuation factor (α_k) takes into account the inverse square dependent path loss, reflection loss etc. The total received signal is

$$f_R(t) = \sum_{k=0}^{N} f_k(t)$$

Intensity of the received signal is given by

$$
\begin{aligned}
Y_R(t) &= |f_R(t)|^2 = f_R(t) f_R^*(t) \\
&= \sum_{k=0}^{N} \sum_{l=0}^{N} \beta_{kl}(t)\, e^{j\omega_0(t_k - t_l)}
\end{aligned}
\tag{3.3}
$$

where

$$\beta_{kl}(t) = \sqrt{\alpha_k \alpha_l} \left\{ A[1 + \mu X(t - t_k)] \right\}^{1/2} \times \left\{ A[1 + \mu X(t - t_l)] \right\}^{1/2}$$

The N^2 terms of Y(t) can be divided into N terms with k=l and N(N-1) terms with k≠l

$$Y_R(t) = \sum_{k=0}^{N} \alpha_k A[1 + \mu X(t - t_k)] + \sum_{k=0}^{N} \sum_{l=0}^{N} \beta_{kl}(t) e^{j\theta_{kl}} \tag{3.4}$$
$$k \neq l$$

where $\theta_{kl}=\omega_0(t_k-t_l)$. θ_{kl} is critically sensitive to excessive path length. The photodetector surface spans many thousands of wavelengths. When this ensemble of receiver sites spread over thousands of wavelengths is considered, θ_{kl} can be considered as a random variable having a uniform distribution for any k and l. Then the total received signal can be expressed as,

$$Y(t) = E\left[Y_R(t)\right] = \sum_{k=0}^{N} \alpha_k A\left[1+\mu x\left(t-t_k\right)\right] + \sum_{k=0}^{N}\sum_{l=0}^{N} \beta_{kl}(t) E\left[e^{j\theta_{kl}}\right] \qquad (3.5)$$

The mathematical expectation evaluated above is equivalent to spatial integration over the photodetector surface. Therefore the second term containing the rapidly fluctuating θ_{kl} term vanishes in the integration, while the first term is approximately constant over the photodetector surface. The second term is equal to zero since, θ_{kl} has a uniform distribution. Conversion of the intensity variations into an electric signal and by removing DC term results in

$$Y(t) = \sum_{k=0}^{N} a_k X\left(t-t_k\right), \qquad (3.6)$$

where a_k is a constant. Thus the whole process can be modelled as a baseband transmission although X(t) is a large bandwidth signal [15].

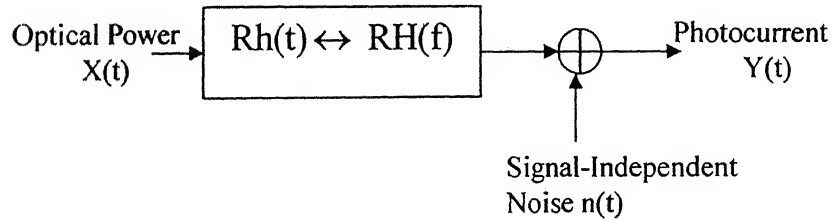The modelling of infrared channel with IM/DD is illustrated in fig. 3.1.

Fig. 3.1(a) **Modelling IR link as a baseband linear, time-invariant system** [10]
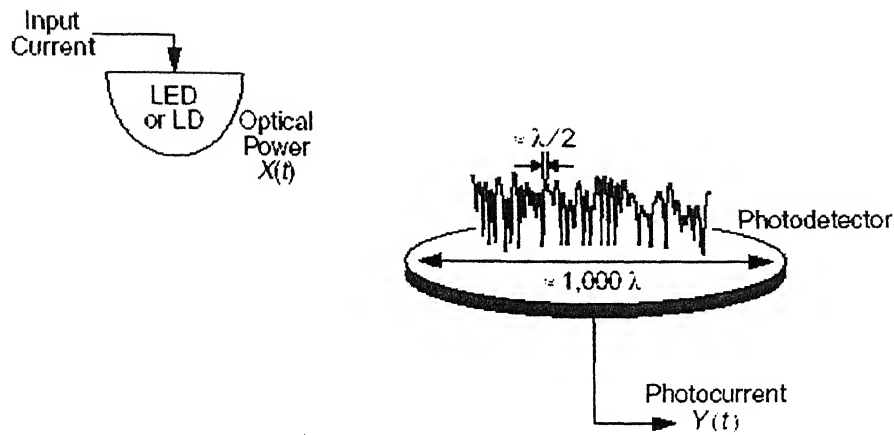
Fig. 3.1(b) **Transmission and Reception of infrared link with IM/DD** [10]

The transmitted waveform X(t) is the instantaneous optical power of the infrared emitter. The received waveform Y(t) is the instantaneous current in the receiving photodetector, which is proportional to the integral over the photodetector surface of the total instantaneous power at each location. The received electric field generally displays spatial variation of magnitude and phase so that "multipath fading" would be experienced if the detector were smaller than a wavelength. This can be seen from fig. 3.1(b). Usually the detector areas are millions of square wavelengths, leading to spatial diversity that prevents multipath fading. Thus even when detector is moved by a distance of the order of a wavelength, no change in channel is observed. But since the transmitted optical power X(t) propagates along paths of varying lengths, infrared channels are subjected to multipath distortion. This is most pronounced in diffuse links. The channel can be modelled as a baseband linear system with instantaneous power X(t), output current Y(t), and an impulse response h(t). This is illustrated in fig. 3.1(a). The linear relationship between X(t) and Y(t) is a consequence of the fact that the received signal consists of many electromagnetic modes.

In most applications, infrared links are operated in the presence of intense infrared and visible background light. Although background noise can be reduced by

optical filtering, it still adds shot noise which is usually the limiting noise source in well-designed receivers. Due to its high intensity, this shot noise can be modelled as white, Gaussian, and independent of X(t). When little or no ambient noise is present, the dominant noise source is the receiver preamplifier noise which is also signal independent and Gaussian. So n(t) is usually modelled as signal-independent and Gaussian. Fluorescent lamps emit infrared that is modulated in nearly periodic fashion; when present, this adds a cyclostationary component to n(t) [1].

The baseband channel model is expressed by [20],

$$Y(t) = RX(t) \otimes h(t) + n(t) \qquad (3.7)$$

where the "$\otimes$" symbol denotes convolution and "R" is the detector responsivity (A/W). The channel input represents instantaneous optical power and so the channel input is non-negative.

$$X(t) \geq 0$$

3.2   IDEALISED DIFFUSE OPTICAL CHANNEL

This section describes the reflection model and some of the properties of the infrared channel. The reflection model usually used in infrared domain is Lambertian. Since a line of sight may not be available, the impulse response may solely depend on the scattered radiation. So there is a great need to correctly characterise the scattering characteristics of the diffuse channel.

3.2.1   Scattering

The infrared channel frequency ranges from 300 GHz upwards. The corresponding wavelength is very small and hence in the infrared domain everything is considered as rough compared to wavelength. The major mechanism which allows communication is reflection of energy. Since the reflecting medium is rough, scattering of light occurs rather than a specular reflection which results in the broadening of scattered energy. The roughness of a surface depends on the material, the wavelength of

incident light and the angle of incidence. The roughness of the surface is reduced as the incident wave comes closer to the normal to the surface, or as the wavelength is made larger. The Rayleigh criterion is often used to calculate whether a surface is rough for a given incidence angle and wavelength. It states that the maximum height of irregularity is defined as [21]

$$\Delta h \ < \ \frac{\lambda}{8\sin\theta_i} \tag{3.8}$$

where λ is the wavelength (m) and θ_i is the incident angle (rad) measured with respect to the surface. This formula is based on the criterion that a scattered component reaching the receiver must exhibit a phase shift less than $\pi/2$ in order for the surface to be considered smooth. In the infrared case, where the wavelength of operation is around 800nm, for normal incidence a surface is rough if $\Delta h > 0.1$ μm. Scattering can be visualised as in fig. 3.2.

Reflection (Smooth Surface)   Scattering (Rough Surface)
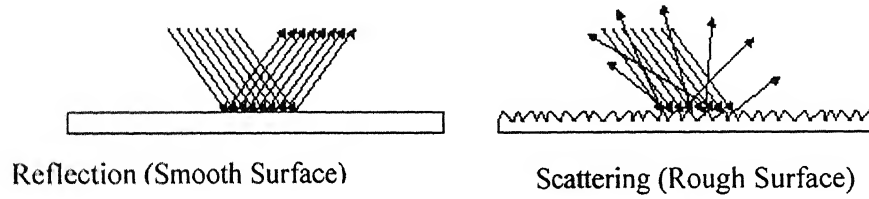
Fig. 3.2   **Reflection Properties of different materials** [2]

One assumption made is that the phase is random. The incident waves on a rough surface travel slightly different lengths to reach the scatterer, since the surface can be visualised like the array of cavities as clear from fig. 3.2. The different length causes phase change in the scattered waves, and phase can be considered random. Inter-reflections also bring about phase change. Hence it is reasonable to assume that the phase of a scattered wave can be modelled as random.

3.2.2   Lambert's Law

In infrared domain, scattering can be characterised by Lambert's law [2], [21] which describes a perfectly rough or diffuse surface. This states that, the reflected

power is proportional to the cosine of the observation angle, making the material a perfect scatterer that transmits radiation towards all directions. The Lambertian model is based on the assumption that infrared radiation follows the laws that describe light instead of electromagnetic waves. Figure 3.3 illustrates a source or a reflector that follows Lambert's law.
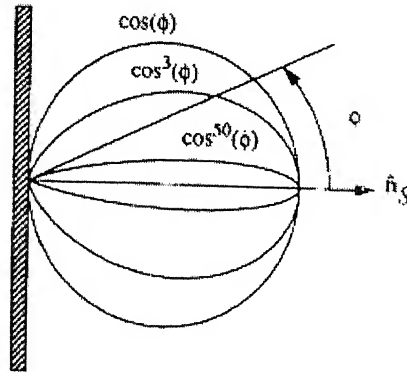
Fig. 3.3 **Lambertian radiation pattern** [8]

In fig. 3.3, $\hat{n}_s$ is the surface normal, ϕ is the observation angle and n describes the directionality of the reflecting material.

Lambert's law gives the radiation pattern of a source or reflecting element and is given by [2], [21]

$$P(\theta) = \frac{n+1}{2\pi} \rho P_s \cos^n(\phi) \qquad (3.9)$$

where n is the mode number of the element, a dimensionless number which describes the directionality and takes values of 1 to any large integer, P_s is the source or incident power in Watts. ρ is the reflection coefficient of the material which is used only when diffuse reflection is calculated. Since in infrared all surfaces are assumed to be rough, for all cases except transmitting elements, n=1. A mode number larger than unity describes the directionality of a source, and it would not be appropriate to increase the mode number of a reflecting element, since this would only concentrate the radiation around the normal of the element. A transmitting element, on the other hand, may have

a high mode number in order to concentrate the transmitted power towards an area of interest. For the reflecting elements, Lambert's law is [2], [21]

$$P(\theta) = \frac{\rho}{\pi} P_s \cos(\phi)$$
(3.10)

In most simulations, the reflections can be characterised by Lambertian model. All the simulations in this work consider the Lambertian reflection model.

3.2.3 Path Loss

At the receiver the power received in an infrared LOS link is given by [ ]

$$P_r = \frac{n+1}{2\pi} \cos^n(\phi) \frac{\cos(\theta)A_R}{R^2} rect(\frac{\theta}{FOV}) P_t$$
(3.11)

where n is the mode number of the source and characterises it directionality, ϕ is the angle between the normal to the transmitter and the line joining the transmitter and the receiver, θ is the angle between the normal to the receiver and the line joining the transmitter and the receiver, A_R is the area of the receiving element measured in m^2, R is the distance from the transmitter to receiver measured in m, FOV is the angle of the field of view (FOV) of the receiver in rad and P_t is the transmitted power in watts. [9] Figure 3.4 gives a pictorial representation of the source and the detector.
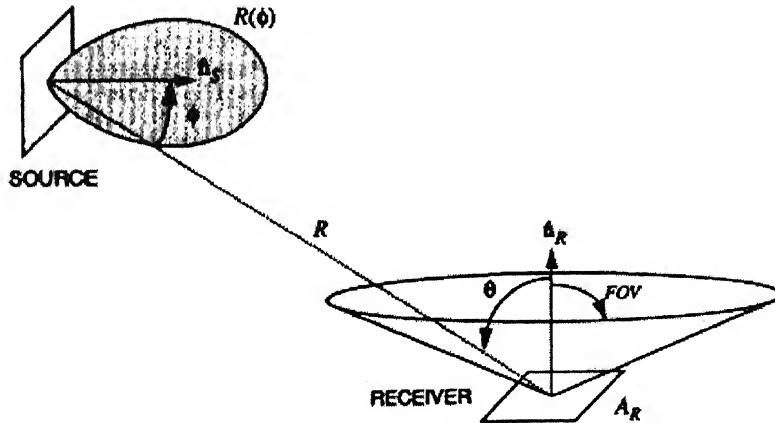

Fig. 3.4 **Source and detector configurations** [9]

In eqn.(3.11)

$$rect(\frac{\theta}{FOV}) = \begin{cases} 1, & if \ |\theta| \leq FOV \\ 0, & if \ |\theta| > FOV \end{cases}$$

The *rect* function ensures that all the rays that fall outside the FOV of the receiving element get rejected. For the above path loss calculation to be valid, the assumption $R^2 >> A_R$ should be satisfied, since the received irradiance must be constant across the photodiode surface.

Although true reflections contain both specular and diffusive components, in this work it is assumed that all reflectors are purely diffusive ideal Lambertian. This assumption gives very accurate results in almost all cases. The mode number is taken to be unity which corresponds to a traditional Lambertian source. The above expression can be suitably modified to find the path loss under any configuration.

3.3 CHARACTERISING INFRARED CHANNELS

The goal of characterising a multipath infrared channel is to determine the average transmitted optical power given by eqn.(3.12), which is required to achieve a certain bit-error rate for a particular modulation scheme.

$$P_t = \lim_{t \to \infty} \frac{1}{2T} \int_{-T}^{T} X(t) dt \qquad (3.12)$$

The impulse response of a channel is fixed for a given position of transmitter, receiver and intervening reflectors within a room, and changes significantly only when any of these are moved by distances of the order of centimetres [1]. The channel is assumed to be time invariant because of the slow movement of people and high bit rates. This means that the channel will vary significantly only on the time scale of many bit periods. The power requirements can be separated into two factors: an **optical path loss** and a **multipath power penalty** [10]

The optical path loss is given by $1/G_0$, where $G_0 = \int_{-\infty}^{\infty} h(t)\, dt$ is the optical gain. Then the received power is

$$P_r = G_0 P_{tx}.$$

$$Optical\ path\ loss\ (dB) = -10\ log_{10}\ G_0. \tag{3.13}$$

A single parameter of the channel impulse response h(t), viz. the normalised delay spread, is an excellent predictor of the multipath requirement. The temporal dispersion of an impulse response can be expressed by the channel rms delay spread τ_{rms}, which can be calculated from [10], [20],

$$\tau_{rms} = \left[\frac{\int (t - \mu)^2\, h^2(t)dt}{\int h^2(t)} \right]^{1/2} \tag{3.14}$$

where 'μ' is the mean delay given by

$$\mu = \frac{\int th^2(t)\, dt}{\int h^2(t)\, dt} \tag{3.15}$$

The limits of integration extend over all time. Since h(t) is fixed for a given configuration, so is the rms delay spread. There is a dimensionless parameter usually defined, the normalised delay spread D_T, which is the ratio of rms delay spread and the bit duration T [10], [22]-[25].

3.4 IMPULSE RESPONSE MODELS

3.4.1 Multiple Bounce Impulse Response Model

Infrared Multipath propagation is dominated by diffuse reflection, a process in which the energy reflected from each surface element follows a Lambertian distribution, independent of the angle of incidence. Barry et.al. [8], [9] have developed a technique to simulate the multipath impulse response taking into account, arbitrary number of reflections from room surfaces. This technique is based on the observation that given a particular source S and a receiver R in a room with reflectors, light from source can

reach the receiver only after many number of reflections. Therefore, the impulse response can be written as an infinite sum [9]:

$$h^{(k)}\left(t;S,R\right)=\sum_{i=1}^{N}h^{(0)}\left(t;S,\varepsilon_{i}\right)\otimes h^{(k-1)}\left(t;\varepsilon_{i},R\right) \tag{3.16}$$

where $h^{k}(t)$ is the response of the light undergoing exactly k reflections. Reflecting surfaces in the room are divided into small elements,ε_{i}, $1\leq$ i $\leq$ N. The kth response can be calculated from the $(k-1)^{th}$ response through this recursive method. Each reflecting element ε_{i} makes a contribution to the k-bounce response that is composed of the LOS response from the source to the element ε_{i} convolved with the (k-1) bounce response between the reflecting element and the receiver.

Although this is the most accurate of all the currently used methods, this requires a lot of computation time as well as resources. This recursive solution is not practical when a fast study of the maximum baud rate reachable and the BER induced by the multipath power penalty are needed. It has been found out that the delay spread of a channel is a remarkably accurate predictor of the ISI induced power penalties. For purposes of evaluating ISI caused by multipath infrared propagation, a functional channel model is developed in [10] by considering a diffuse link consisting of a Lambertian transmitter that is directed towards a diffuse reflector of infinite extent, and a receiver co-located with the transmitter. This is called as the Ceiling bounce model. In this thesis, ceiling bounce model is used as one of the bases for the study of infrared channel.

3.4.2 Functional Modelling Of Multipath Dispersion: The Ceiling Bounce Model [10]

The impulse response due to diffuse reflection from a single infinite plane reflector can be used as a good model for characterising infrared channel. The infinite Lambertian reflecting plane is chosen, as it is a good approximation to a large ceiling. The general expression is very complex involving complicated integrals. But for the

case in which the transmitter and receiver are co-located, this takes a simplified closed form [10],

$$h(t) = \frac{c\rho A H^4}{\pi} \frac{\frac{ct}{2} u\left(t - \frac{2H}{c}\right)}{\left(\frac{ct}{2}\right)^4 \left(\frac{ct}{2}\right)^4} = \frac{2^7 \rho A H^4}{c^6 \pi t^7} u\left(t - \frac{2H}{c}\right)$$ (3.17)

where ρ is plane reflectivity, A is receiver photodiode area, H is the height of the ceiling above transmitter and receiver and c the velocity of light.

This can be simplified to [10],

$$h(t) = G_o \frac{6a^6}{(t+a)^7} u(t)$$ (3.18)

which defines the ceiling bounce model for multipath dispersion.

Here, $a = 12\sqrt{\frac{11}{13}}\tau_{rms}$, $G_0 = \frac{\rho A}{3\pi H^2}$ represents the optical gain, and u(t) the Heaviside's unit function.

The 3-dB cut off frequency for the ceiling bounce model is given by

$$f_{3dB} = \frac{0.925}{4\pi\tau_{rms}}$$ (3.19)

3.4.3 Statistical approach for the approximation of rms delay spread

In [11], [12], the author speaks of a statistical approach to the problem of estimating the channel impulse response in a diffuse wireless infrared channel. In this approach, rms delay spread is estimated by testing its dependence on the propagation characteristics. From the studies done by P.Jimenez *et.al.* [11], [12] it has been proved that the rms delay spread depends mainly on the distance between the emitter and reflector (d_{err}), the transmission angle between emitter and receiver (θ), and the mode number n of emitter radiation pattern. Fig. 3.5 gives the system set up generally considered. We have used this approach in some of our simulations.
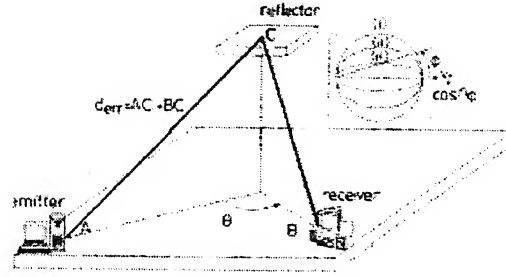
Fig. 3.5 **System considered to estimate rms delay spread** [11]

The general expression for rms delay is given by

$$\tau_{rms}(ns) = a + b\cos(c\theta + d) \tag{3.20}$$

For ensuring uniform power distribution, it is assumed that both the transmitter and receiver points towards the centre of the ceiling. Then the delay spread can be rewritten in terms of the propagation characteristics specified above as

$$\tau_{rms} = -0.82n^{0.03} + 0.58n^{-0.11}d + (-0.54 + 0.19d)\cos(0.019\theta - 0.32) \tag{3.21}$$

Another possible configuration is obtained if both emitter and receiver are pointing vertically to the ceiling. Fig. 3.6 shows this configuration. We used this configuration in this study. In this case, the rms delay spread is,

$$\tau_{rms} = -2.37 + .007n + (0.8 - .002n)d \tag{3.22}$$

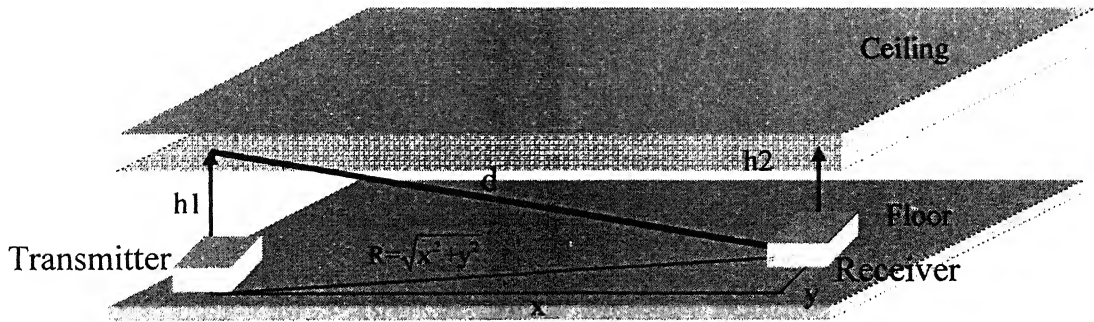where n is the mode number and d is the distance between transmitter and receiver in three dimensional space.

Fig. 3.6 **Configuration considered for delay spread calculation**

3.5   INFRARED CHANNEL DC GAIN

The frequency responses of infrared channels are relatively flat near dc, so channel dc gain G_0 is one of the important parameters to characterize the channel. It relates the transmitted and received average powers by,

$$P_r = G_0 P_t \qquad\qquad (3.23)$$

Diffuse infrared links exploit the fact that a wide variety of common building materials are efficient diffuse infrared reflectors. In 800-900nm range, typical plaster walls and acoustical ceiling tiles have diffuse reflectivities in the range 0.6-0.9. Most building materials are approximately Lambertian reflectors. To compute the dc gain of diffuse channels, one must consider the effect of multiple reflections from surfaces within the room. An approximate value can be found out by considering only the first bounce off the ceiling, which is assumed to be a Lambertian reflector of reflectivity ρ [1]. Consider the configuration given in fig. 3.7.
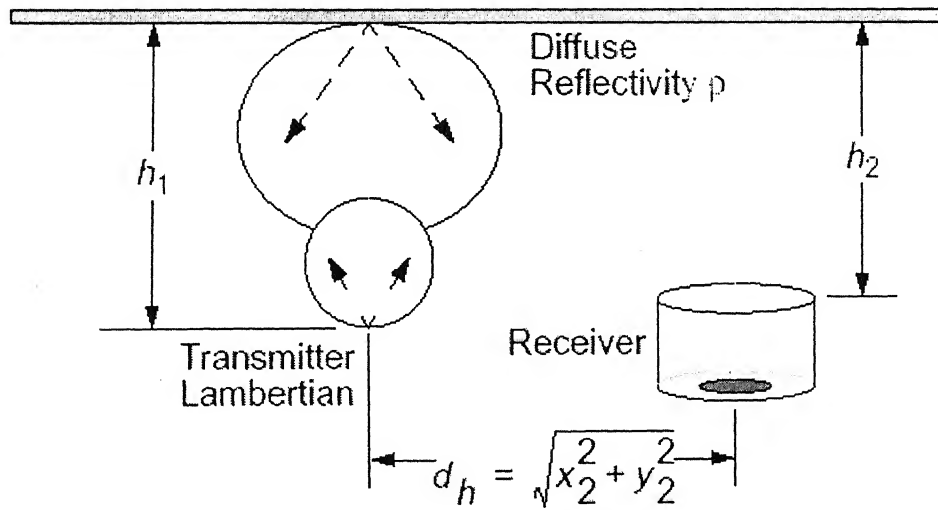

Fig. 3.7 **Configuration chosen for DC gain calculation** [1]

It is assumed that the transmitter is pointed straight upward and emits a Lambertian pattern. The receiver is also pointed straight upwards. The transmitter and receiver are located at co-ordinates (x_1, y_1) and (x_2, y_2), respectively, in the horizontal (x, y) plane and h_1 and h_2 represents the transmitter-ceiling and receiver-ceiling vertical separations,

respectively. Considering an infinite ceiling, the power reflected from each ceiling element is integrated to obtain the expression [1], [17]

$$G_0 = \frac{\rho A_R h_1^2 h_2^2}{\pi^2} \iint\limits_{ceiling} \frac{dxdy}{\left(h_1^2 + (x-x_1)^2 + (y-y_1)^2\right)^2 \left[h_2^2 + \left(x-x_2\right)^2 + \left(y-y_2\right)^2\right]^2} \quad (3.24)$$

The expression assumes a detector field-of-view half angle of 90° and a Lambertian source. The results almost follow closely the experimental results, but it shows variations at large horizontal separations, where the effect of neglected higher order reflections is relatively important.

The path loss can be easily derived from the DC Gain as

$$\text{Diffuse path loss (optical dB)} = -10 \log_{10} (G_0) \quad (3.25)$$

3.6 RECEIVER SNR AND BER

It is assumed that the receiver transmits at a bit rate R_b using OOK. If P_r is the received power, then $P=H(0)P_t$. The signal to noise ratio is given by [1]

$$SNR = \frac{(RP_r)^2}{\sigma_{total}^2} = \frac{A^2}{\sigma_{total}^2},$$

where σ_{total}^2 represents the noise variance,

$$\sigma_{total}^2 = \sigma_{shot}^2 + \sigma_{thermal}^2$$

and R gives the responsivity of the photodiode. A is taken as the average received optical power. Assuming shot noise to be dominant,

$$SNR = \frac{(RP_r)^2}{\sigma_{shot}^2} = \frac{A^2}{\sigma_{shot}^2} \quad (3.26)$$

The shot noise variance is given by, $\sigma_{shot}^2 = 2qP_n I_2 R_b$, where P_n is the background noise power and I_2 is the noise-bandwidth factor [1].

Bit error rate is given by,

$$BER = Q\left(\sqrt{SNR}\right), \quad (3.27)$$

where Q is the Gaussian Q function defined by,

$$Q(x) = \frac{1}{\sqrt{2\pi}} \int_x^\infty e^{-t^2/2} dt = \frac{1}{2} erfc\left(\frac{x}{\sqrt{2}}\right)$$

Thus the above eqn (3.27) clearly shows the dependence of SNR and hence, bit error rate on background noise power and data rate [1], [20], [26].

3.7 MULTI-PATH INDUCED POWER PENALTY

Non-directed infrared channels can be modelled as fixed, linear systems with additive Gaussian noise. As explained in sections 3.3 and 3.4, the channel exhibits multipath distortion that can cause inter symbol interference(ISI) in high bit rate links. When the ISI is relatively mild, it leads to an optical power penalty, but if it is severe, it may lead to a BER floor.
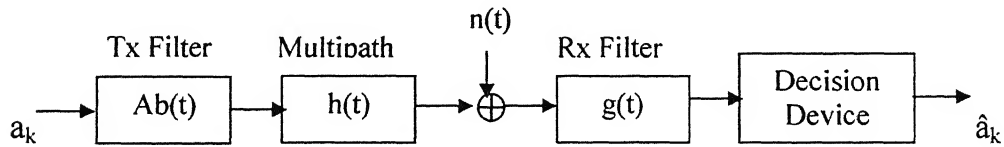

Fig. 3.8 **Baseband OOK System** [8], [9].

Consider a baseband OOK system as shown in fig. 3.8. The symbols $a_k \in \{0,1\}$, are passed through a transmit filter with impulse response Ab(t) at a bit rate of 1/T, where A is proportional to the average optical intensity of the transmitter. The output of the transmit filter, which represents the intensity of the transmitted signal, is passed through the multipath channel with impulse response h(t). A is taken as the average received optical power. The additive noise n(t) represents the shot noise due to ambient light and can be modelled as a Gaussian random process. At the receiver end, there is a matched filter with response g(t). Both b(t) and g(t) are assumed to have area T. The received signal plus additive noise passes through this filter at the receiver. At the receiving end, sampling is done at the bit rate, quantised and $\hat{a}_k$, the estimate of the kth bit is obtained [8], [9].

At the receiving side,

$$y_k = Aa_k \otimes h_k + n_k \qquad (3.28)$$

where $\otimes$ denotes convolution and h_k is the equivalent discrete-time impulse response

given by

$$h_k = b(t) \otimes h(t) \otimes g(t)\big|_{t=kT} \qquad (3.29)$$

and n_k is given by

$$n_k = n(t) \otimes g(t)\big|_{t=kT} \qquad (3.30)$$

The optimum threshold adopted for error detection is A/2. The discrete time impulse

response can be rewritten as

$$h_k = h_0 \delta_k + (1 - \delta_k) h_k \qquad (3.31)$$

where δ_k is a unit impulse and $(1-\delta_k) h_k$ represents the impulse response tail.

For a given sequence of bits $a_k \equiv (...a_{k-2}, a_k, a_{k+1}...)$, the probability that the kth bit

estimate $\hat{a}_k$ is in error is given by

$$\Pr[error | a_k] = Q\big(\chi(1 - X_k)\big), \qquad (3.32)$$

where Q is the Gaussian Q function and $\chi \equiv A/(2\sigma)$, σ^2 is the variance of noise and X_k

represents ISI given by,.

$$X_k = 2 \sum_{i \neq k} a_i h_{k-i} \qquad (3.33)$$

The total bit error rate can be found by averaging over all possible bit sequences:

$$BER = E\big[Q\big(\chi(1 - X_k)\big)\big] = \frac{1}{2^M} \sum_a Q\left(\frac{A}{2\sigma}\left(1 - 2\sum_{i \neq k} a_i h_{k-i}\right)\right) \qquad (3.34)$$

$$= \frac{1}{2^M} Q\left(\frac{A}{2\sigma}(2h_0 - 1)\right) \qquad (3.35)$$

where M is the length of the impulse-response tail. [8], [9], [17]

If there was no multipath dispersion, then X_k would be identically zero and BER would

reduce to $Q(\chi)$. The value of χ required to achieve a desired BER of BER_0 would then

be $\chi_0 = Q^{-1}(BER_0)$. Due to dispersion, a large value of χ is required to achieve BER_0. Multipath power penalty can be defined as the increase in optical signal power required to overcome ISI and maintain the same BER as a link transmitting over an ideal, nondispersive channel having the same path loss, and using a matched receiver filter [17]

$$Power\ Penalty\ = 10\ \log_{10}\left(\frac{\chi\ required\ for\ BER_0}{Q^{-1}(BER_0)}\right)dB \qquad (3.36)$$

$$= 10\ \log_{10}\left[\frac{Q^{-1}(2^M\ BER_0)}{(2h_0-1)Q^{-1}(BER_0)}\right] \qquad (3.37)$$

In order to calculate power penalty, we can use the following closed form expression [11]

$$Power\ Penalty\ =\ 10\ \log_{10}\left[\frac{Q^{-1}(2^M\ BER_0)}{\left(1-\frac{2\tau_{rms}}{T}\right)Q^{-1}(BER_0)}\right]dB\ , \qquad (3.38)$$

T being the period of data.

The above expression clearly shows that the multipath power penalty can be estimated from normalised delay spread (τ/T) value. When normalised delay spread is equal to 0.5, the power penalty becomes infinite. For low BERs, τ/T must be less than 0.5.

3.8 PROPOSED MODIFIED APPROACH FOR CALCULATING IMPULSE RESPONSE

In this section we propose a modified approach for calculating the impulse response of diffuse channels. The steps of this approach are listed below.

- We chose the configuration used in the standard ceiling bounce model with the transmitter and receiver pointing vertically to the ceiling. In this configuration, the RMS delay spread depends upon the distance between the transmitter and

receiver and separation from the ceiling only. The system is assumed to be perfectly diffuse.

- The RMS delay spread is calculated using the statistical approach explained in section 3.4. RMS delay spread is found out using the closed form expression given in eqn. (3.22).

- Pathloss is found out by the numerical integration of eqn. (3.24). Path loss is calculated for different transmitter and receiver positions.

- From the estimated delay spread and path loss, the impulse response of the channel is calculated using Ceiling bounce model. In the conventional ceiling bounce modeling approach [10], the authors first assume a co-located transceiver system and calculate the impulse response. Then a complicated correction procedure is done to reach the final accurate solution. We propose a method to eliminate the computational burden in the traditional approach. The RMS delay spread calculated using statistical approach and the pathloss evaluated by the integration is used directly in the ceiling bounce model. The results obtained agree very well with the results of recursive approach.

- Frequency response of the system can be found out by taking the Fourier transform of the impulse response, This gives the system bandwidth for different configurations.

Thus, using the above procedure any diffuse infrared system can be properly characterised using its impulse and frequency responses.

CHAPTER 4

COMPUTATION OF CHANNEL PARAMETERS

The aim of the thesis is to investigate the different propagation properties of the indoor optical wireless diffuse channel. This chapter gives the details of the simulation studies done and detailed discussion of results. The effect of transmitter and receiver location on different system features viz., RMS delay spread, pathloss and multipath power penalty are analysed in detail.

In the analysis, we have used our modified Ceiling bounce approach (section 3.8) as the base model. As explained in section 3.8, RMS delay spread and channel path loss are calculated initially. A detailed study of their dependence on transceiver position is performed. Then the impulse response is obtained using the modified approach. The frequency response is calculated from the impulse response to get the system bandwidth. The variation of system bandwidth with respect to location is analysed in detail. In the later sections, a study is done on the dependence of background noise and received power level on the BER. Following that, the multipath power penalty due to dispersion is calculated assuming a tolerable BER and its dependency on the location is further investigated.

One corner of the room is assumed to be the origin (0,0) in all the simulations. The length of the room is assumed to be the x co-ordinate, breadth to be the y co-ordinate and height to be the z co-ordinate. The influence of the horizontal distance between transmitter and receiver and their separation from the ceiling on rms delay spread is studied in the following section.

4.1 EFFECT OF TRANSMITTER AND RECEIVER POSITION ON RMS DELAY SPREAD

The rms delay spread variations with different transmitter and receiver position in three rooms (5mX5mX3m, 5.5mX6mX3.5m and 10mX10mX3m) are calculated. Two cases are considered in each room. In the first case, transmitter is kept at one corner of the room and receiver is moved all over the room. The second case considers transmitter to be placed at the centre of the room and receiver, moved all around the room. Figs. 4.1 to 4.6 show the variation in the delay spread with transmitter and receiver location. Consider fig. 4.1. The room size is 5mX5mX3m and the transmitter is at the origin. Minimum value of rms delay spread is found to be 2.43 ns when the transmitter and the receiver are at the same place, i.e. at the corner. The maximum value is 6.16 ns when the receiver is at the diagonally opposite corner. Figs. 4.2 and 4.3 show the variation of rms delay spread with distance (between transmitter and receiver) in the two other rooms of larger size than the first. We see that the maximum value of rms delay spread increases with room size. This is because of the increase in the number of paths and the path lengths which causes more time to reach the destination after multiple reflections. When the room size is 10mX10mX3m, the value of delay spread is 11.57 ns which is much larger than that of the first case. In figs. 4.4 to 4.6, the transmitter is kept at the center of the room. If we consider the value of the maximum rms delay spread in the first case (fig 4.4), we find that its only 3.73 ns which is less than the maximum value obtained for the case when transmitter was at the origin. The same trend can be observed in the two other cases also. This shows that the value of rms delay spread depends on the position of transmitter, receiver and the room size chosen. Even in the same room, by properly locating transmitters, we can reduce the rms delay spreads.
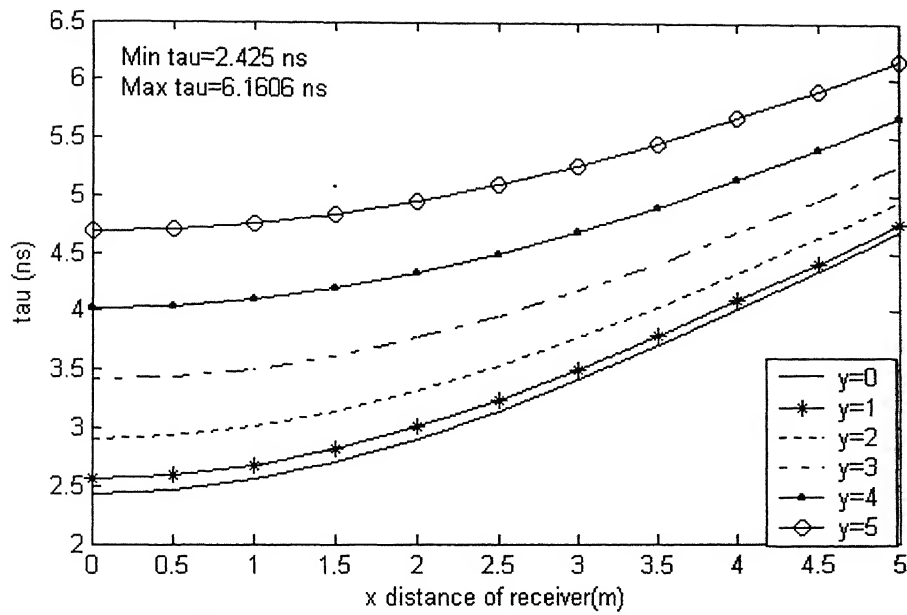
Fig. 4.1 **Variation of rms delay spread with receiver position
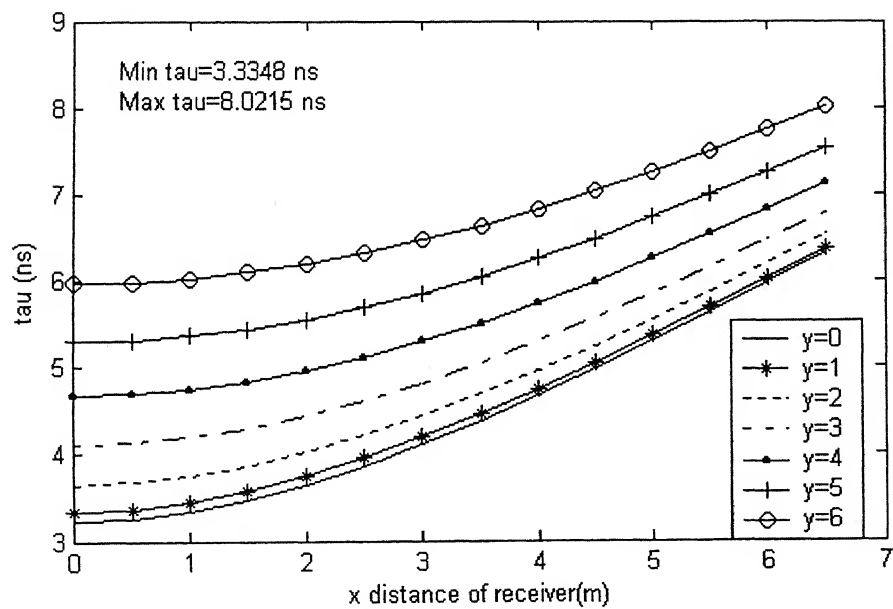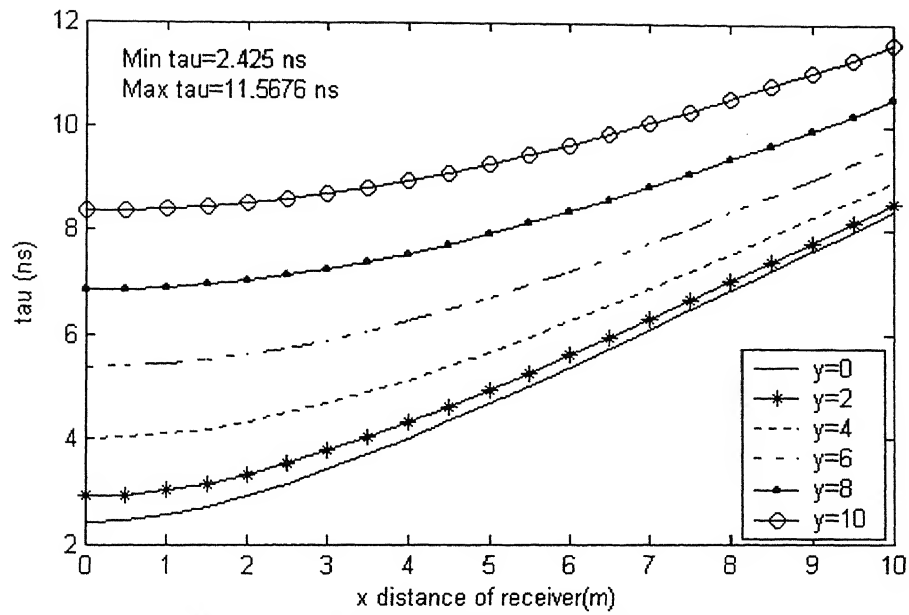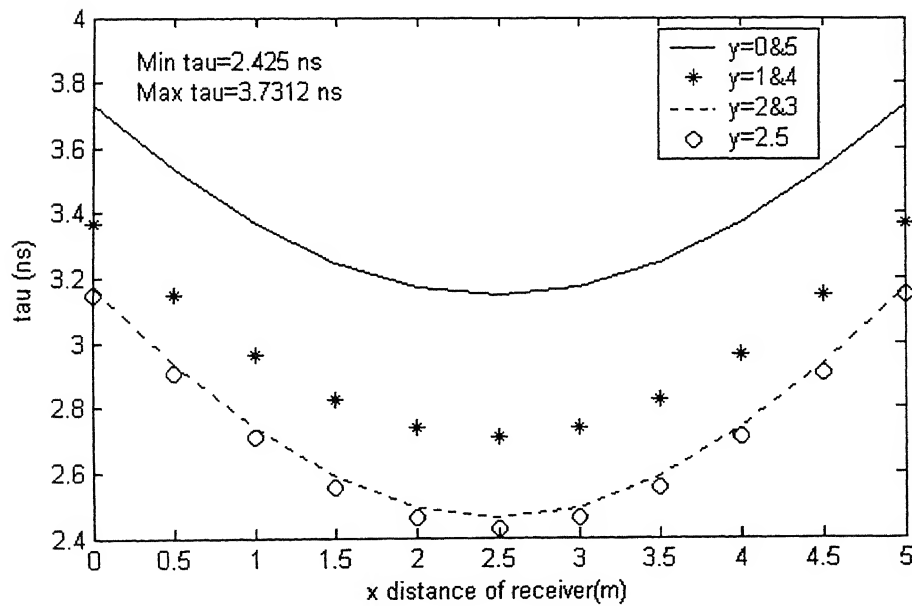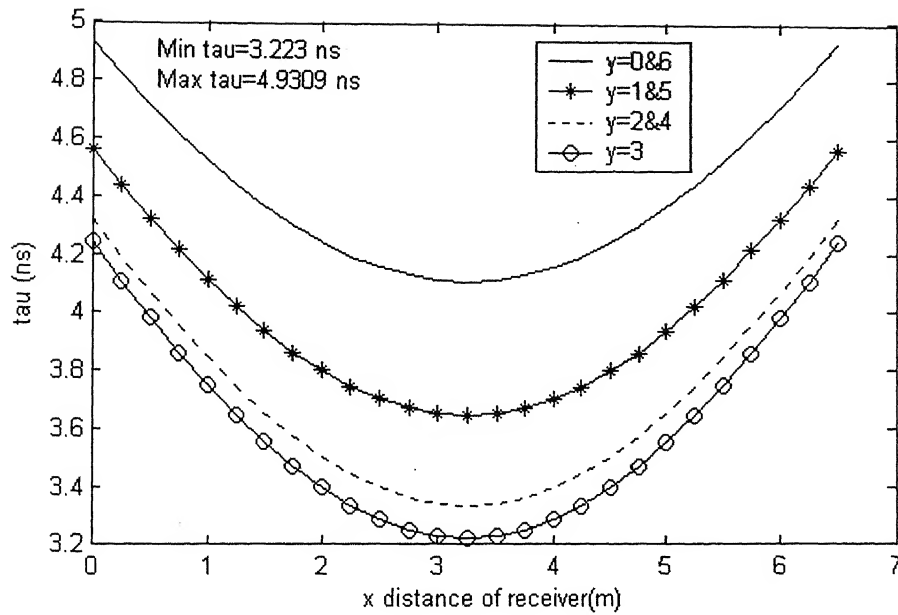Room size 5X5X3 & Transmitter at one corner of the room**

Fig. 4.2 **Variation of rms delay spread with receiver position
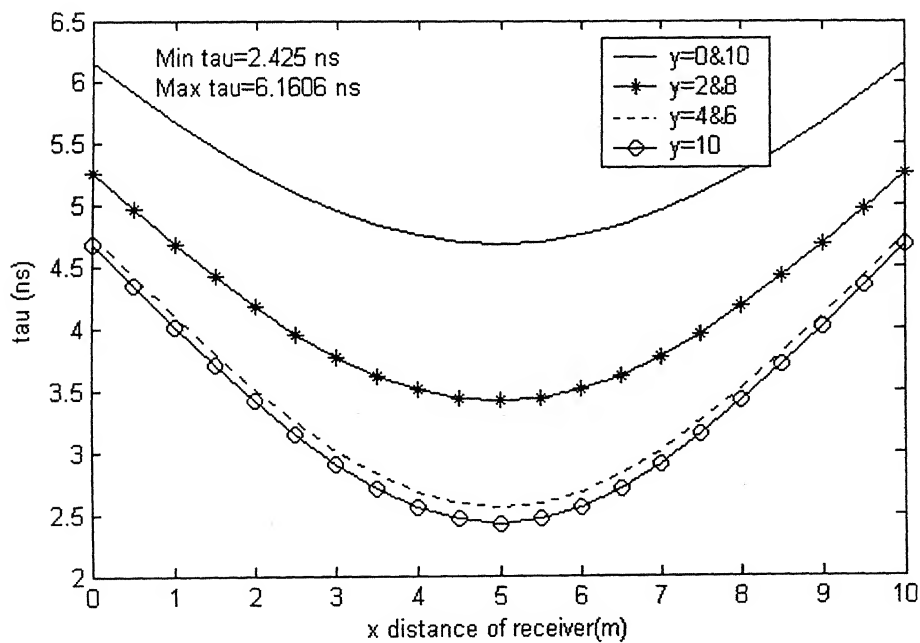Room size 6.5X6X3.5 & Transmitter at one corner of the room**

Fig. 4.3 **Variation of rms delay spread with receiver position**
Room size 10X10X3 & Transmitter at one corner of the room

Fig. 4.4 **Variation of rms delay spread with receiver position**
Room size 5X5X3 & Transmitter at the center of the room

Fig. 4.5 **Variation of rms delay spread with receiver position**
Room size 6.5X6X3.5 & Transmitter at the center of the room

Fig. 4.6 **Variation of rms delay spread with receiver position**
Room size 10X 10X3 & Transmitter at the center of the room

From figs. 4.1 to 4.6 it is clear that the value of rms delay spread depends only on the distance between the transmitter and the receiver, as well as the separation from the ceiling. It increases with increase of both the quantities. If d is the horizontal separation

between the transmitter and receiver, then the variation of rms delay spread with separation can be represented as given in fig. 4.7. Fig. 4.8 shows the effect of both the horizontal and vertical separations on rms delay spread.
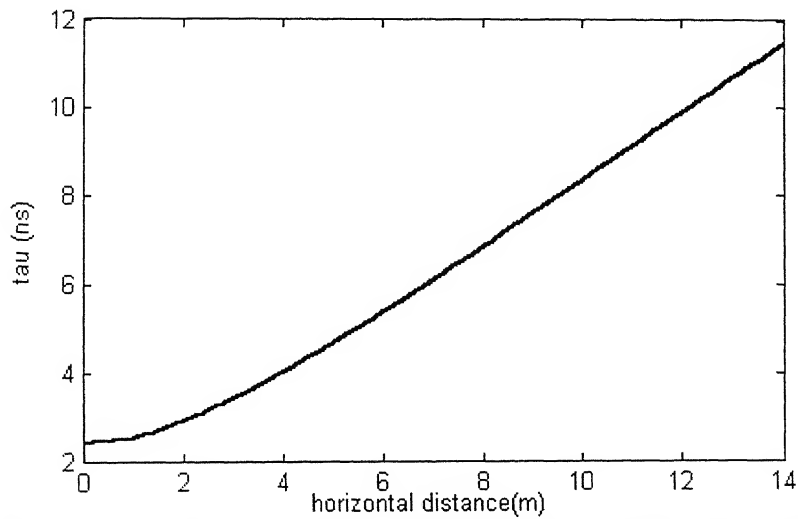

Fig. 4.7 **Variation of rms delay spread with horizontal separation between transmitter and receiver.**
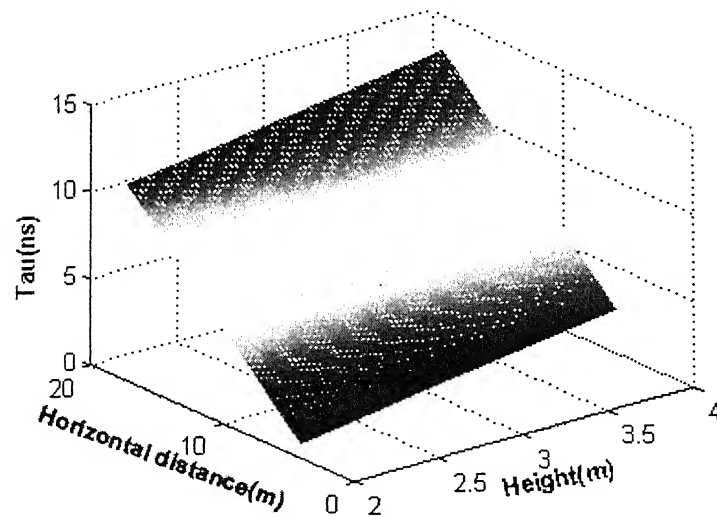

Fig. 4.8 **Variation of rms delay spread with horizontal separation between transmitter and receiver and separation from ceiling**

4.2 EFFECT OF TRANSMITTER AND RECEIVER POSITION ON PATH LOSS

The path loss variation in a room of size 5mX6mX3m is calculated for different positions of transmitter and receiver and plotted. The graphs show the variation in path loss with distance. DC gain and path loss are calculated using equations (3.27) and (3.28) through numerical integration. Their dependence on the location of the transmitter and receiver is studied.
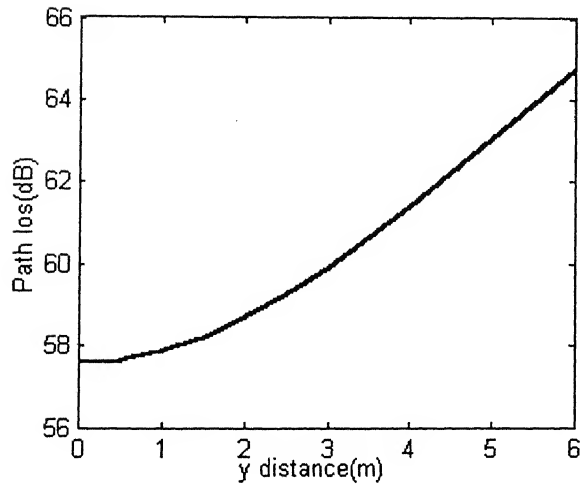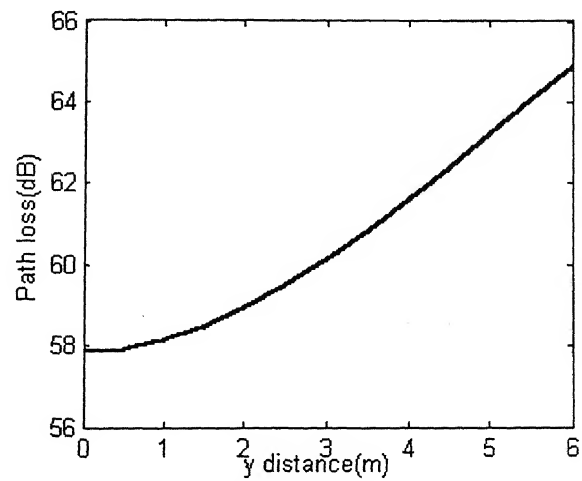

Fig. 4.9 (a) Receiver x distance= 0

Fig. 4.9 (b) Receiver x distance= 1

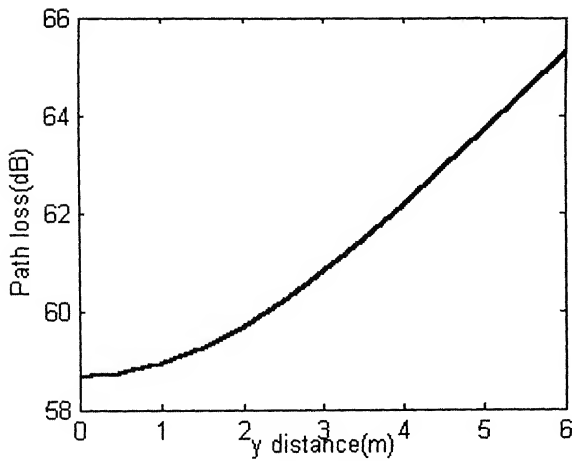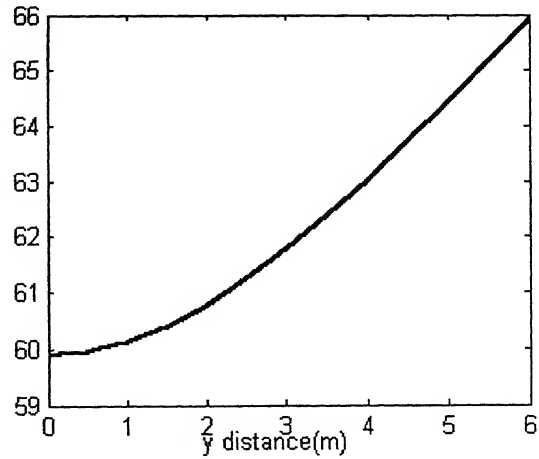Fig. 4.9 (c) Receiver x distance=2
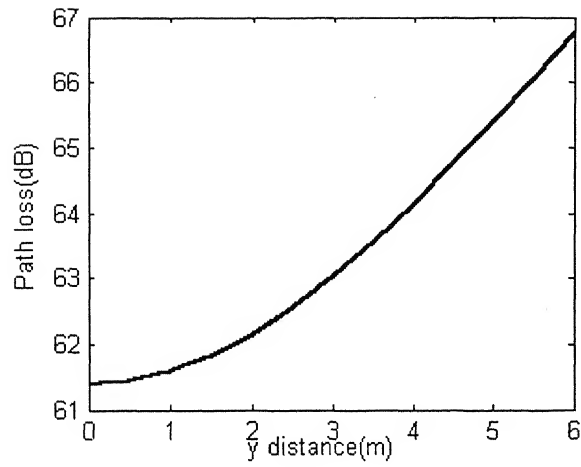
Fig. 4.9(d) Receiver x distance= 3
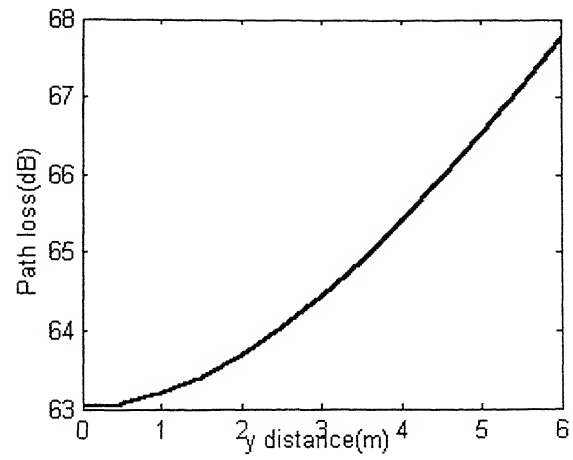
Fig. 4.9(e) Receiver x distance= 4   Fig. 4.9(f) Receiver x distance= 5

Fig. 4.9 (a)- 4.9(f) **Variation of path loss with position in a room keeping transmitter at one corner of the room and moving receiver all over the room.**
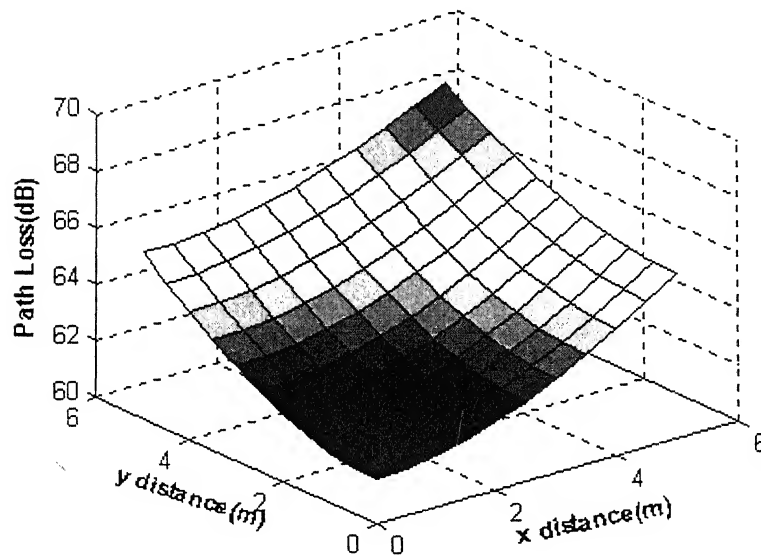

Fig. 4.10 **Variation of path loss with position of receiver in a room of size 5mX6mX3m**

Figs 4.9 and 4.10 show the variation of path loss with the position of transmitter and receiver. These figures clearly show that, when the separation between the transmitter and receiver increases, path loss also increases. The numerical integration technique (Refer appendix A) used above considers only a single bounce from the ceiling. It neglects the higher order reflections. At less separation this does not create significant error. When the separation increases, the actual path loss is less than the loss calculated using this technique. This is because; the higher order reflections become more significant at larger distances. Up to 5m separations, the path loss estimated using this approach is fairly accurate. But for separations more than that, it does not give a very accurate result although we can get a rough idea of the range of power obtained. If very accurate results are required, one should go for more complicated recursive methods. The power estimated using this approach would be only around 80% of the actual power at a particular location. Fig. 4.11 gives a power profile distribution in a room of size 5mX6mX3m. The transmitted power is assumed to be 1watt.
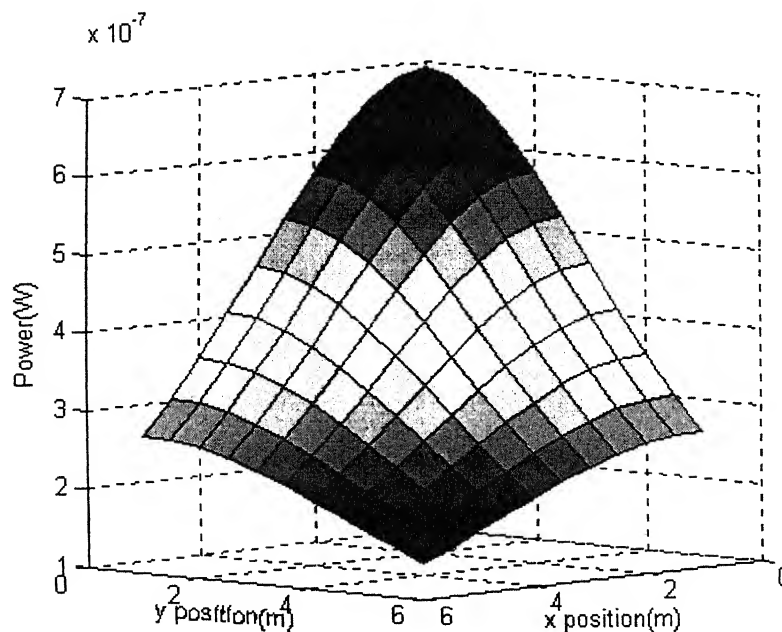

Fig. 4.11 **Power distribution in a room of size 6X6X3, assuming 1W transmitted power**

4.3 SIMULATION OF IMPULSE RESPONSE AND MAGNITUDE RESPONSE USING CEILING BOUNCE APPROACH

Having calculated the rms delay spread and path loss, the impulse response can be easily found out using ceiling bounce model (eqn.3.18). The DC gain and rms delay spread found out earlier are used as the two parameters in the ceiling bounce model expression. The model thus obtained, predicts exactly the impulse response at any location. In the conventional ceiling bounce approach, the component $h_c(t) = \dfrac{6a^6}{(t+a)^7} u(t)$ is found out by adjusting the parameter 'a' properly considering the position of the transmitter and receiver. This is a complicated process. In this work, first $h_c(t)$ is found out using the exact rms delay spread calculated by the relatively simple process in section 4.1. Then this impulse response estimate is modified using the path loss calculated in section 4.2. The values obtained shows similarity with those obtained using Barry's recursive method.

The complete impulse response is found out using $h(t) = G_o h_c(t)$. No further corrections are to be made. Since all the higher order reflections may not be considered, this will not be as efficient as Barry's method. But the advantage here is the reduction in computational complexity and simulation time without loosing much accuracy.

The magnitude response of the infrared channel for a particular configuration can be found out from the impulse response by taking its Fourier transform. The magnitude response gives an estimate of the maximum data rate which can be allowed for a particular configuration. By studying the effect of location on the 3dB frequency, the maximum data rate for a certain room size can be predicted with good degree of accuracy. The impulse response and corresponding magnitude response for some of the room configurations are shown in figs. 4.12 and 4.13

Fig. 4.12(a)
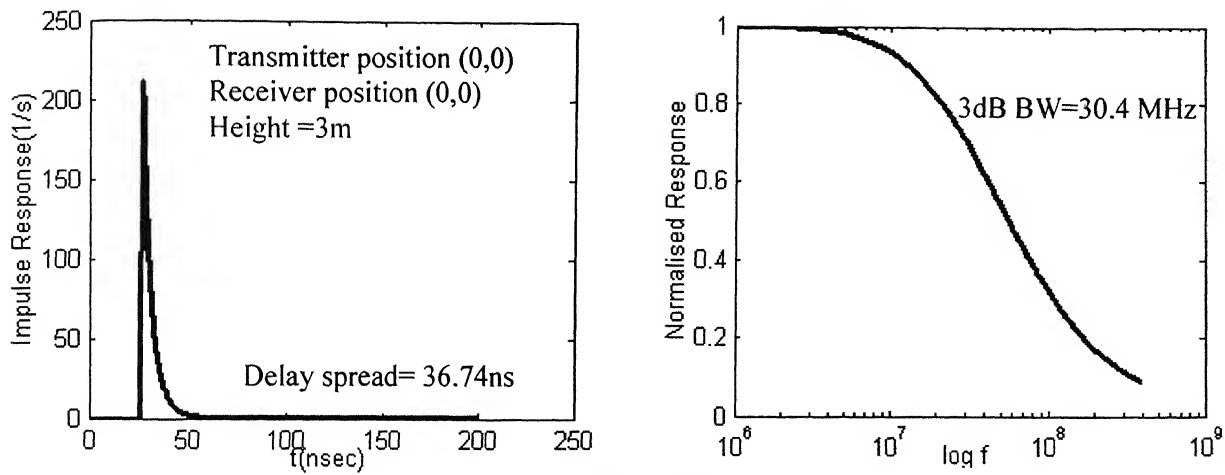

Fig. 4.12(b)

Fig. 4.12(c)

Fig. 4.12(a) - 4.12(c) Impulse Response and Frequency Response of the channel
for   different transmitter and receiver positions for a room size 5mX5mX3m

Fig. 4.13(a)

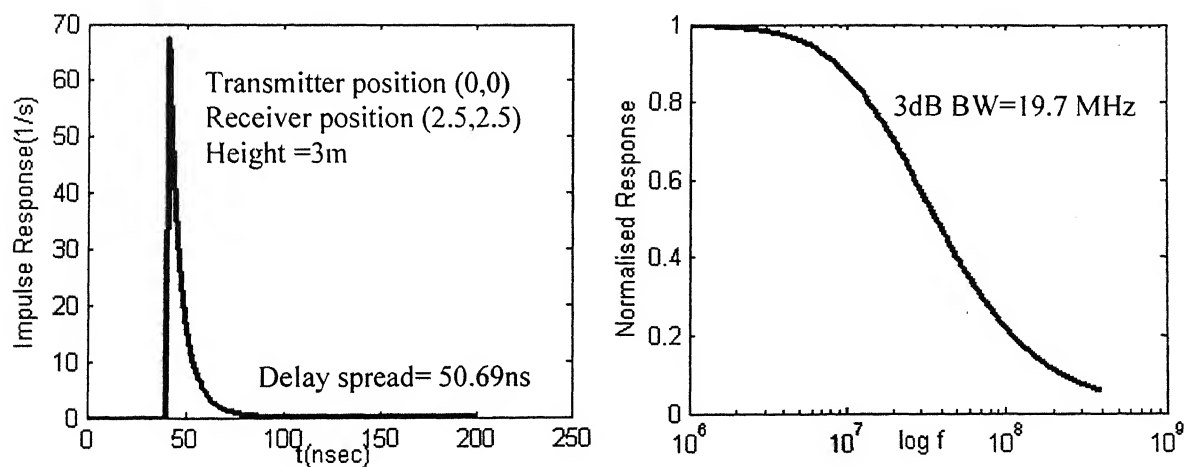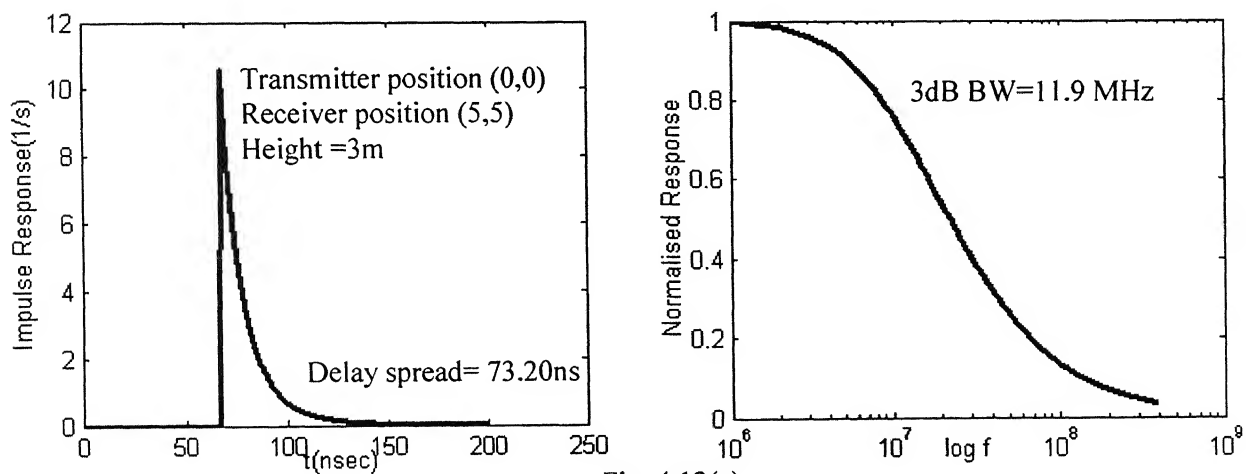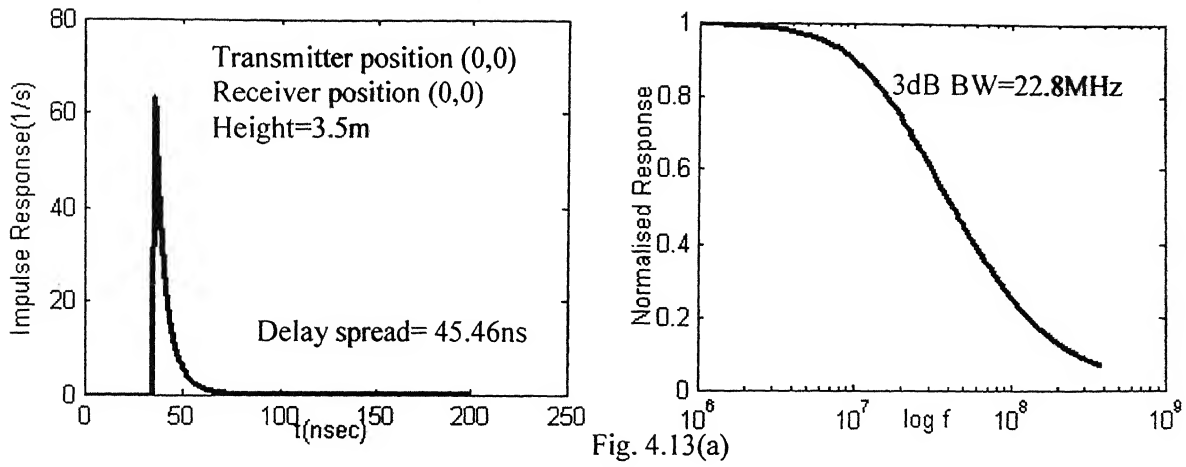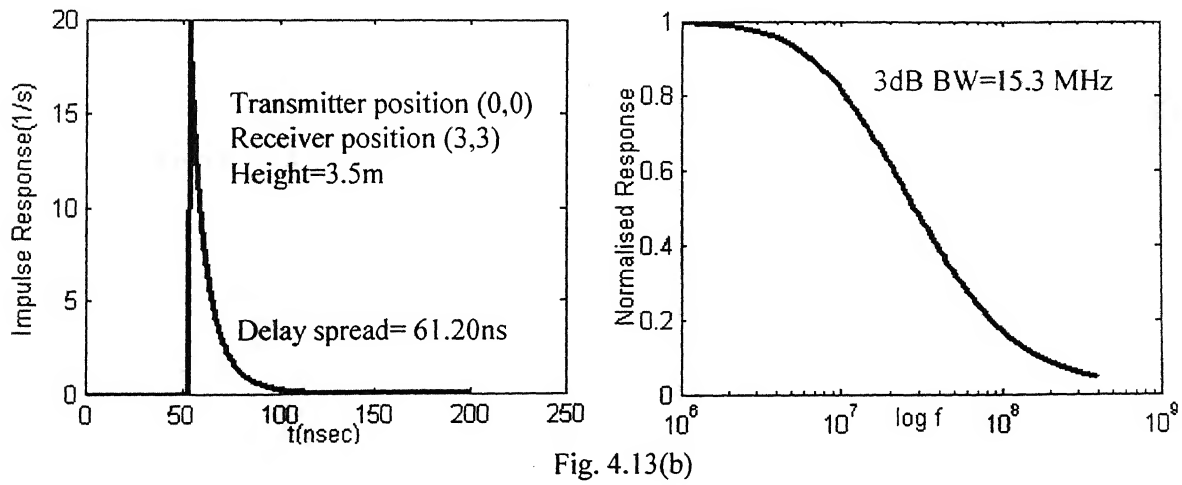Fig. 4.13(b)
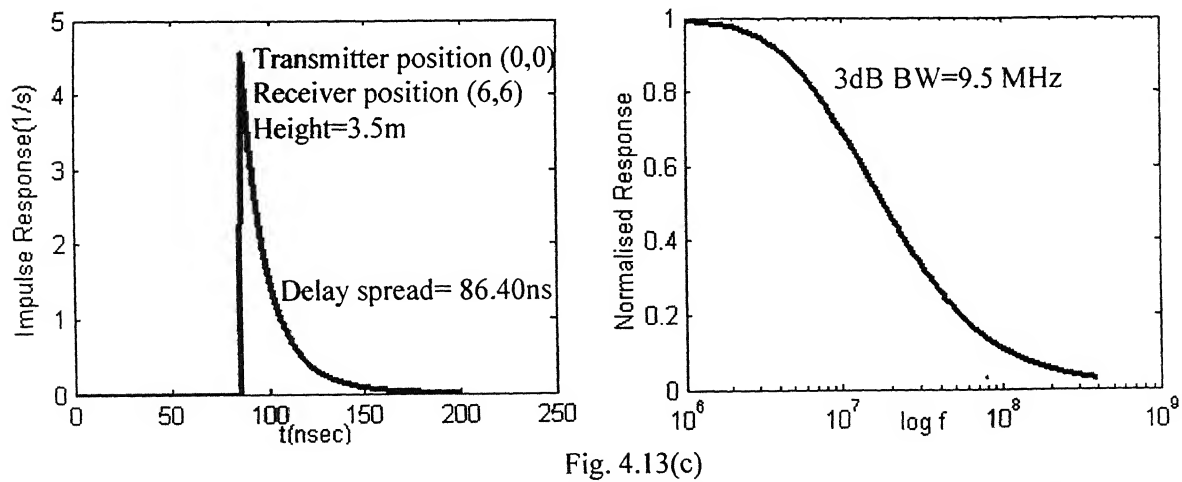
Fig. 4.13(c)

Fig. 4.13(a) - 4.13(c) **Impulse Response and Frequency Response of the channel for different transmitter and receiver positions for a room size 6mX6mX3.5m**

Figs. 4.12 and 4.13 show the variation in the channel impulse response and the frequency response with the Tx-Rx configuration in the room. Fig. 4.12(a) to 4.12(c) give the impulse and frequency response variations within a room of dimensions 5mX5mX3m for three positions of the receiver, (0,0,0), (2.5,2.5,0), (5,5,0), respectively. Similarly fig. 4.13(a) to 4.13(c) show the impulse and frequency response variations within a room of dimensions 6mX6mX3.5m, at the three receiver positions (0,0,0), (3,3,0), (6,6,0), respectively.

From the impulse response plots it is clear that, when the distance between the transmitter and receiver is increased, the amplitude of the impulse response decreases, while the delay spread increases, and vice versa. The same trend is noticed when the separation from the ceiling is changed. Ideally the impulse response should be a single infinitesimally narrow pulse. But due to multi path propagation, it widens and becomes wider and wider as the path length increases. This is evident from the plots in fig.4.12 and 4.13. The variation in impulse response spread with separation between the transmitter and receiver can be represented in a single plot as shown below in fig. 4.14,

Fig. 4.14 **Effect of horizontal separation between transmitter and receiver on impulse response**

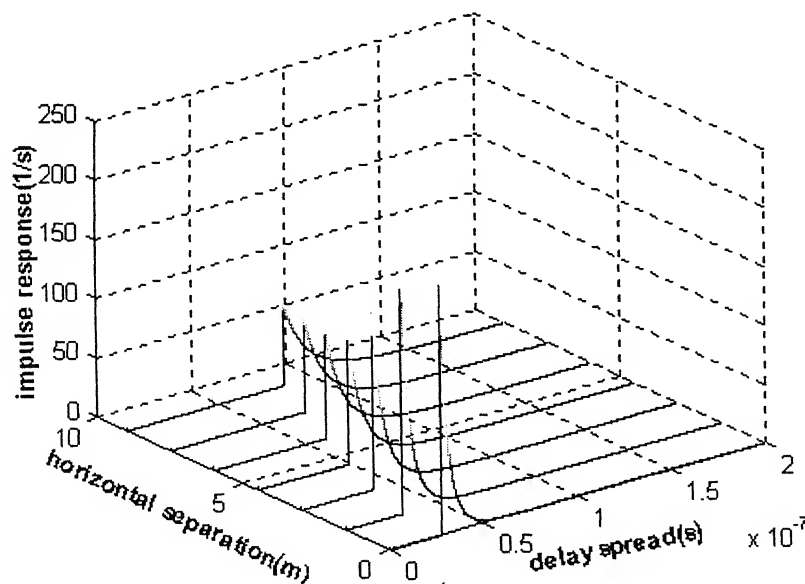where the impulse response is plotted against the horizontal separation between the transmitter and receiver and the delay spread of the response. From the plot it can be seen that, the amplitude of the response decreases as the separation increases. This is because of the increase in path loss which results in the reduction of total power received. The delay before the initial pulse also increases with increase in separation, because of the increase in distance for the first reflection off the ceiling. Also, the plot gets wider as the separation is increased from 0 to 10m. When the distance between transmitter and receiver increases, there is an increase in the number of multi paths and also path length. This causes the impulse response to spread out more as is evident from fig. 4.14.

The frequency response plots from fig.4.12(a) to 4.13(c) show the variation in the system bandwidth with Tx-Rx configuration. Consider fig. 4.12(a) and 4.13(a). For the same horizontal configuration of the transmitter and receiver, the 3dB bandwidths are 30.4MHz and 22.8MHz for room sizes 5mX5mX3m and 6mX6mX3.5m, respectively. The reduction in bandwidth for the second configuration is due to the increase in the ceiling separation. If the three plots at three different positions in the same room are taken, we see that there is wide variation in the bandwidth. Consider fig. 4.12(a) to 4.12(c). It can be seen that the system bandwidth varies from 30.4MHz to 11.9MHz. As the separation between the transmitter and receiver increases, the system bandwidth also decreases. This has effect on the maximum bit rate achievable. The maximum bit rate that can be used for transmission is more if receiver is near to the transmitter since the transmission path length is less then. With distance, the multipath effect more and more pronounced which causes a decrease in the bandwidth, thus resulting in reduction of the maximum bit rate achievable. For OOK modulation, the maximum bit rate achievable is the system bandwidth[ ]. So when very high bit rates compared to the bandwidth are used, it results in inter symbol interference resulting in the degradation of bit error rate. The factors affecting bit error rate are studied in the next section.

4.4 EFFECT OF BACKGROUND NOISE AND RECEIVED SIGNAL POWER ON BIT ERROR RATE

In this section, the receiver SNR (considering only shot noise) and BER are computed assuming that the receiver transmits OOK signals at a rate R_b. Eqns. 3.26 and 3.27 give the dependence of bit error rate on the background noise, received signal power, and bit rate.

Fig. 4.15 **Variation of SNR with frequency for different Background noise level =0.5mW**
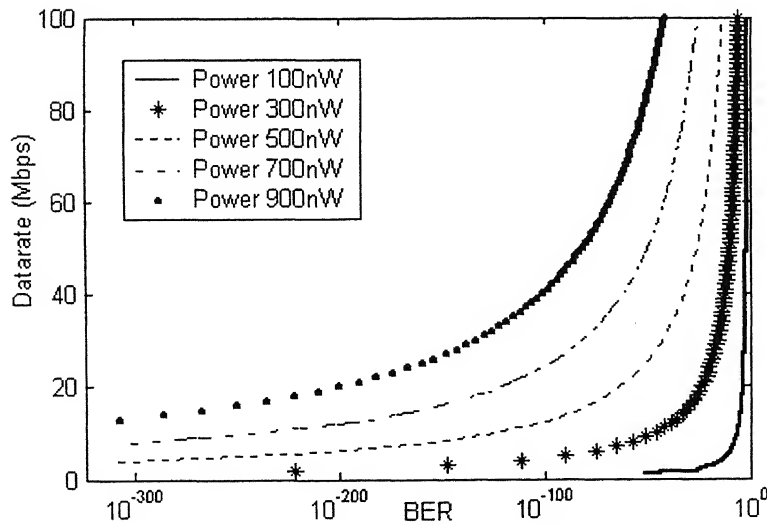
Fig. 4.16 **Variation of BER with frequency for different Background noise level =0.5m**

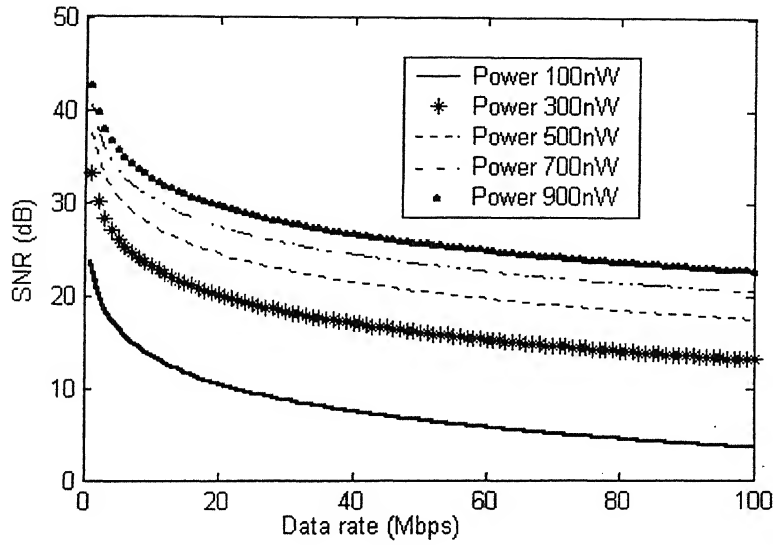Fig. 4.17 **Variation of SNR with frequency for different Background noise level =1mW**

Fig. 4.18 **Variation of BER with frequency for different Background noise level =0.5mW**
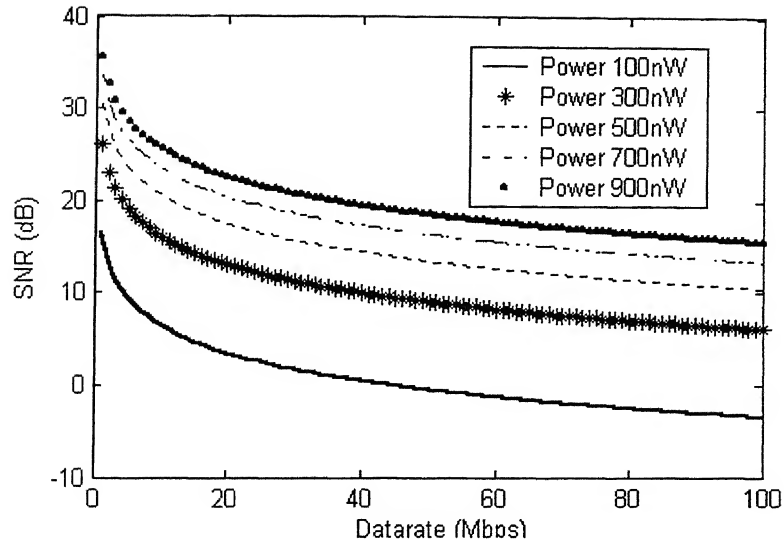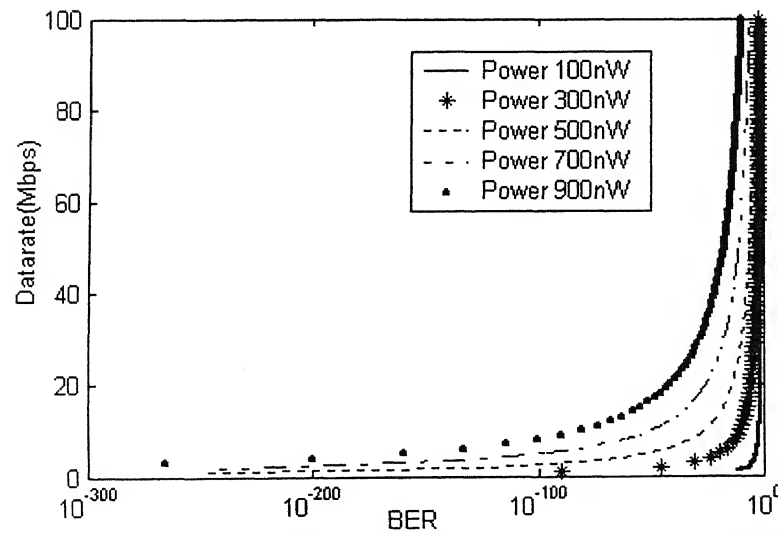
Figs. 4.15 to 4.18 show variation of signal to noise ratio and bit error rate with frequency for different received powers and background illumination (ambient light). When the received power is 100nW, the maximum data rate that can be used for a

BER<10^{-6} is only 10Mb/s for a background illumination of 0.5mW. The corresponding SNR is 13.5dB. If the background illumination is 1mW, the maximum data rate that can be used reduces drastically to 1Mb/s. If received power is 300nW, up to a bit rate of 40Mb/s the BER is tolerable (BER<10^{-6}), provided the background illumination up to 0.5mW. The SNR also is 13.5dB for 40Mb/s. In the same case, if background illumination is made 1mW, the maximum data rate tolerable is only 8Mb/s. For the received power values 900nW and 700nW, the SNR is more than 13.5 dB for all the frequencies and hence the BER is less than 10^{-6} up to 100Mb/s. For 500nW of received power, if the background noise is 0.5mW, data rates up to 100Mb/s come in the tolerable range. For 1mW background illumination, the maximum data rate possible is less than 50MHz.

Thus the above graphs show the sharp fall in the maximum possible data rate when the received power decreases. When the horizontal separation increases, the power received decreases due to increase in path loss. This causes a sharp fall in SNR and BER at high data rates.

The noise level depends on the amount of background illumination present. At data rates up to 100Mb/s, only the shot noise is dominant. When higher ranges are explored, the thermal noise due to the amplifier components and other stray parameters also become more dominant. In the above analysis, we see that the data rate achievable is depended very much upon the background noise level also. When the noise level increases from 0.5mW to 1mW, the data rate falls sharply.

4.5 ESTIMATION OF POWER PENALTY DUE TO MULTI PATH DISPERSION

Having characterized the multi path channel completely using the channel DC gain and rms delay spread, multi path power requirement can be found out using the eqn.3.36. The power penalty to be tolerated in order to prevent inter symbol interference

in infrared channel using OOK modulation is plotted for different frequencies and positions in figs. 4.19 to 4.22. The tolerable bit error rate is taken as 10^{-6}.

Fig. 4.19 **Multi path power penalty for different receiver positions with respect to frequency for room size 5mX5mX3m**

Fig. 4.20 **Multi path power penalty for different receiver positions with respect to normalised delay spread for room size 5mX5mX3m.**
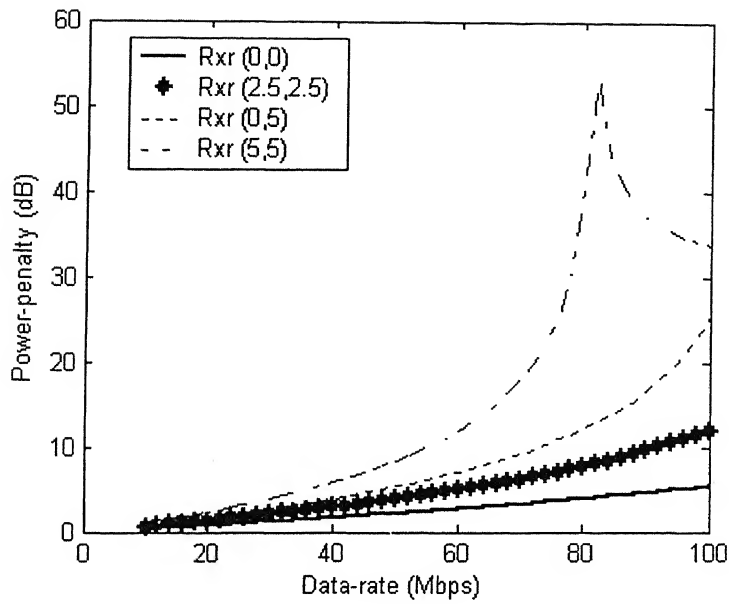
Fig. 4.21 **Multi path power penalty for different receiver positions with respect to frequency for room size 6mX6mX3.5m**
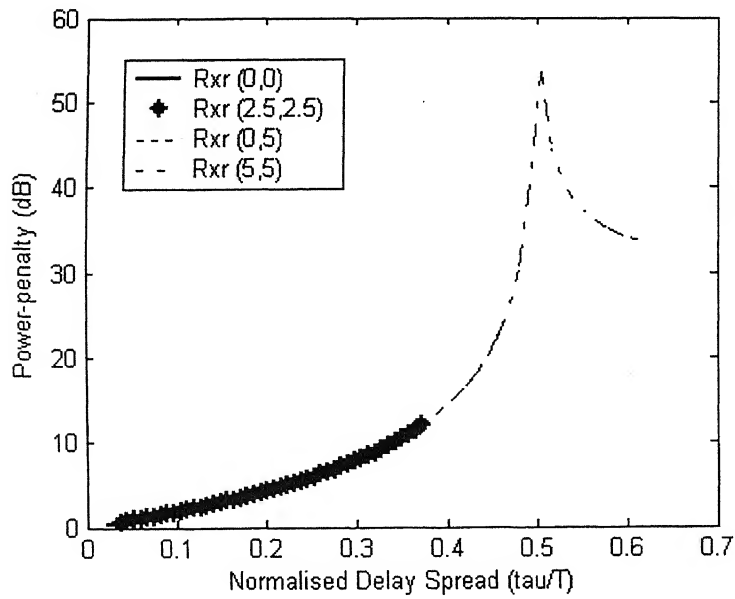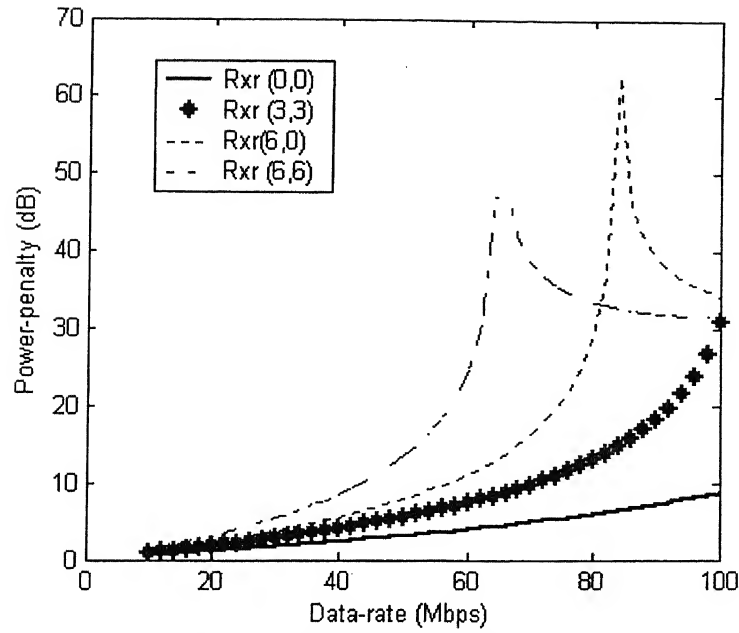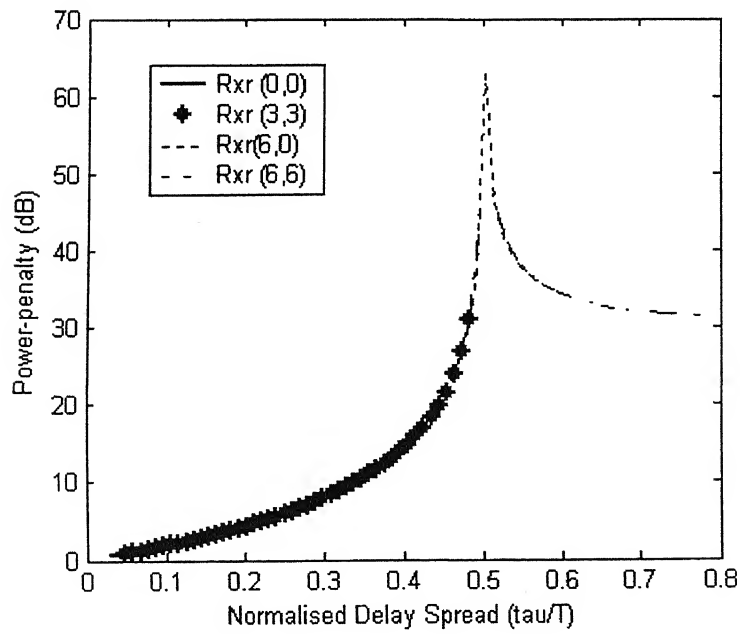

Fig. 4.22 **Multi path power penalty for different receiver positions with respect to normalised delay spread for room size 6mX6mX3.5m.**

Figs. 4.19 and 4.21 show the power penalty versus frequency relation for different room configurations and positions. If we check the power penalty variation at different locations of the room configuration used in fig. 4.19, we observe the following features: The power penalty increases with frequency in all the cases. The only difference is in the rate of increase. This depends on the amount of dispersion at each location. If we take the four locations considered, i.e., (0,0), (2.5,2.5), (0,5), (5,5), for each location the cut off frequency obtained in section 4.3 are 30.4MHz, 19.7MHz, 15.7MHz and 11.9MHz respectively. The power penalty variation also shows a variation with some correlation to these values. For all the cases, the value of power penalty for frequencies nearer to cut off is around 1.2dB which is a tolerable value. After the cut off frequency, the excess power value increases and it goes to higher values at higher frequencies and is difficult to achieve. Similarly, for the configuration used in fig. 4.21, the cut off for the locations, (0,0), (3,3), (6,6) are 22.8MHz, 15.3MHz, 9.5MHz, respectively. The values of multi path power penalty for frequencies below the cut off values for the corresponding locations are less than 1.2dB. Thus in both the configurations we note that, for data rates below the bandwidth of the system, the power penalty due to multi path is less than 1.2dB. Once we go to high data rates compared to the bandwidth, excess power required to keep the BER within limits increases rapidly.

Figs. 4.20 and 4.22 show the variation of power penalty with normalised delay spread for different configurations. It shows clearly, that when the normalised delay spread increases, the power penalty increases. The increase is more for larger transmitter-receiver separation, as well as ceiling separation distances. All these are clearly depicted in the two figures.
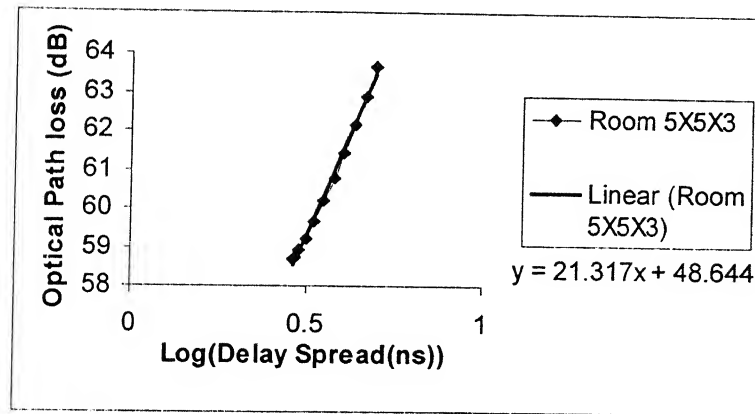
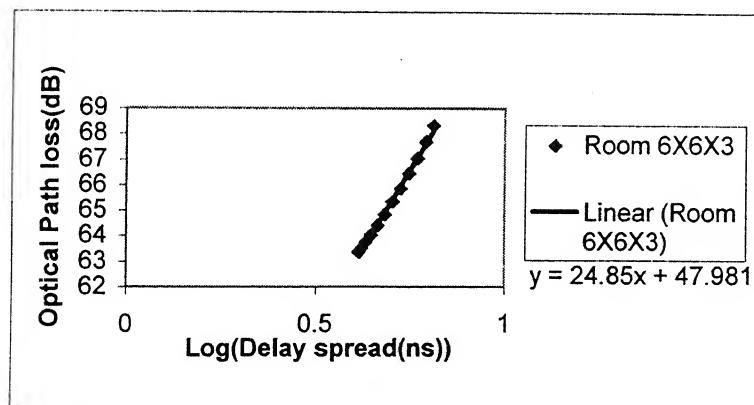Fig. 4.23 Delay spread v/s Path loss (Room 5X5X3)

Fig. 4.24 Delay spread v/s Path loss (Room 6X6X3.5)
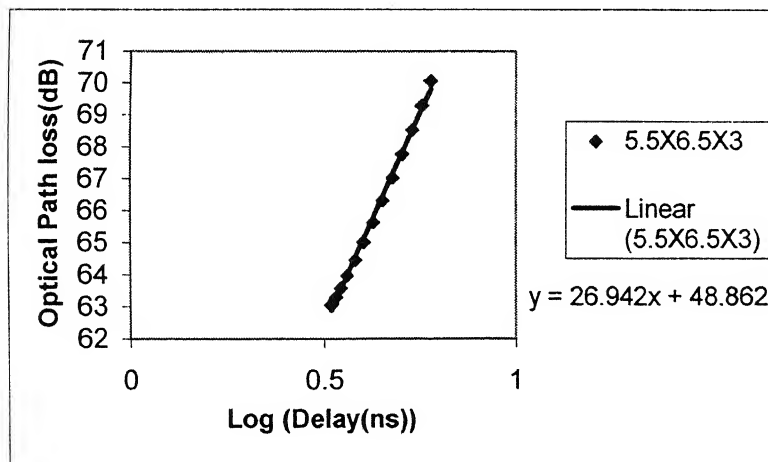
Fig. 4.25 Delay spread v/s Path loss (Room 5.5X6.5X3)

Figs. 4.23 to 4.25 also show the result of a linear regression between the two parameters as a solid line on the plot. The path loss and RMS delay spread for each position are tabulated in Table 4.1. Each row corresponds to a certain y position of the receiver, and the x position varies from zero to the length of the room. The relationship can be represented as $PL=\alpha \log_{10}(\tau)+\beta$, where PL is the path loss and τ is the delay spread. The relationship was obtained in all the positions of all the three configurations. Values of α and β are not same in all cases and depend on the position and configuration. But for most of the cases the values are close as can be seen from Table 4.1.

Room	y position	α	β	Corr.Coeff.	Fit to line
A1	0	18.665	50.176	0.9947	0.9894
A2	1	19.393	49.766	0.9955	0.991
A3	2	21.317	48.644	0.9971	0.9943
A4	3	23.891	47.052	0.9985	0.997
A5	4	26.624	45.241	0.9993	0.9985
A6	5	29.205	43.409	0.9997	0.9993
B1	0	20.801	50.803	0.9953	0.9907
B2	1	21.34	50.441	0.9959	0.9917
B3	2	22.804	49.436	0.997	0.9941
B4	3	24.85	47.981	0.9982	0.9964
B5	4	27.133	46.285	0.999	0.998
B6	5	29.397	44.522	0.9995	0.9989
B7	6	31.488	42.814	0.9997	0.9995
C1	0	20.877	52.639	0.9926	0.9853
C2	1	21.058	52.534	0.9929	0.9859
C3	2	22.382	51.754	0.9948	0.9897
C4	3	24.529	50.434	0.997	0.9939
C5	4	26.942	48.862	0.9984	0.9968
C6	5	29.264	47.254	0.9992	0.9985
C7	6	31.326	45.735	0.9996	0.9993

Table 4.1 **Correlation coefficient between channel delay spread and path loss in different rooms for different positions**

The table shows the correlation coefficient between PL and τ for different configurations. A1 to A6 denote the different room positions in room of size

5mX5mX3m, B1 to B7 of 6mX6mX3.5m, and C1 to C7 5.5mX6.5mX3m. The value of correlation coefficient is greater than 0.99 for all the configurations and positions. Thus we can conclude that at all positions in a room, the delay spread and path loss is highly correlated. Using the numerical results reported in the table, it can also be concluded that the channel delay spread of any room configuration can be approximately estimated from path loss by using,

$$\tau \approx 10^{\left[\left(PL-\beta_{avg}\right)/\alpha_{avg}\right]}$$

where β_{avg} and α_{avg} are the mean values of all the configurations. Using these values, the delay spread can be estimated to a certain extent of accuracy for most cases.

CHAPTER 5

EXPERIMENTAL SYSTEM

In this chapter, an experimental set up for characterisation of indoor infrared diffuse channels is proposed. Some of the experiments done using this set up and the results are also explained and modifications to be done are suggested.

5.1 EXPERIMENTAL CHARACTERISATION OF INDOOR INFRARED CHANNELS

The design of wireless communication systems using an infrared signal carrier requires extensive knowledge about the behaviour of an indoor infrared channel. This requires channel measurements under different conditions and using different optical configurations. The aim of the experimental characterisation is to measure the propagation parameters of intensity modulated directed detection diffuse infrared channel under different configurations. Such measurements could eventually lead us to an in depth understanding of the channel behaviour under different circumstances.

In the experiment conducted, the channel is excited with sinusoidal signal of constant amplitude over a wide range of frequencies. The received power is computed for each frequency component at the receiver side. The frequency response is obtained by varying the frequency of the signal at the transmitter under program control in pre-defined intervals. The whole process of transmission of signal and received signal analysis is automated. From these measurements, the attenuation caused by the channel or the path loss and the 3dB bandwidth of the system can be calculated. The impulse response can be calculated by taking the inverse Fourier transform of the frequency response.

5.2 EXPERIMENTAL SET UP

The experimental set up consists of a transmitter, a receiver and a prototype of a typical room (wooden model) with dimensions 50cmX50cmX30cm. Fig. 5.1 shows the complete circuit diagram of the transmitter and receiver part.
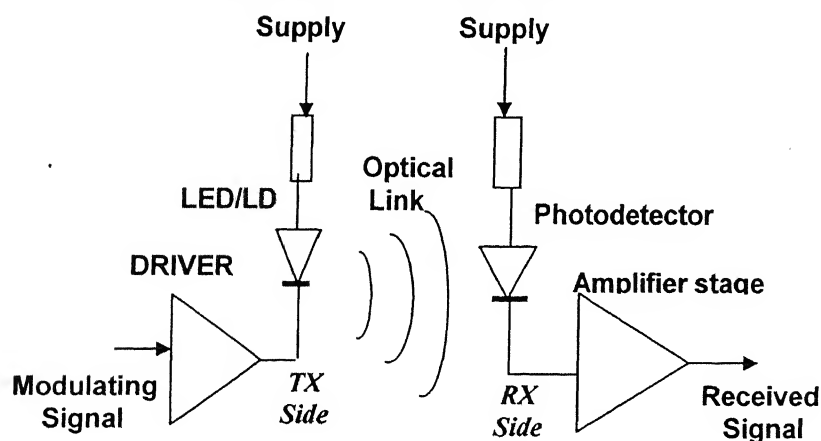
Fig 5.1 **Experimental set up for the characterisation of infrared channel**

The transmitter part consists of an infrared source which will be either laser diode or LED and proper driving circuits. The modulating signal is obtained from a high frequency signal generator (controlled by a PC through GPIB), which gives a constant amplitude sinusoidal signal, which is then converted into the optical domain using a transmitter. The electric signal from the signal generator directly modulates the intensity of the light emitted by the IR source. It is then transmitted through the infrared channel for reception.

The receiver consists of a photodiode and an amplifying stage to achieve good signal to noise ratio of the measured signal. The received signal is viewed on an oscilloscope connected to the controlling PC through GPIB. Detailed explanations of the transmitter, and the interfacing are given in the next sections. Fig. 5.2 gives the block diagram of the complete measurement set up.
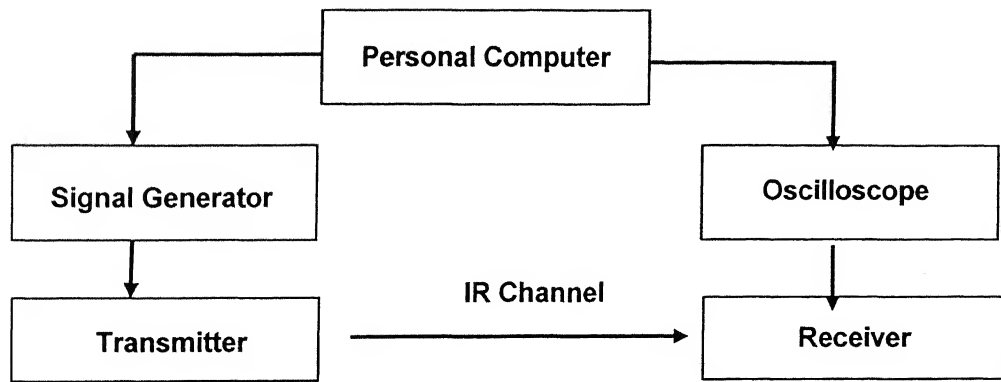
Fig. 5.2 **Block diagram of the complete measurement set up.**

5.2.1 Transmitter side

The transmitter consists of an infrared source, in the present work it is an infrared light emitting diode (IRLED) which is biased properly. The diode is intensity modulated using sinusoidal signal from a high frequency signal source (Agilent 8648A 100KHz-1GHz). The IRLED emits light whose intensity is proportional to the modulating sinusoidal voltage. In the experiments conducted, the average transmitted power level is 3dBm. Fig. 5.3 shows the transmitter circuit.
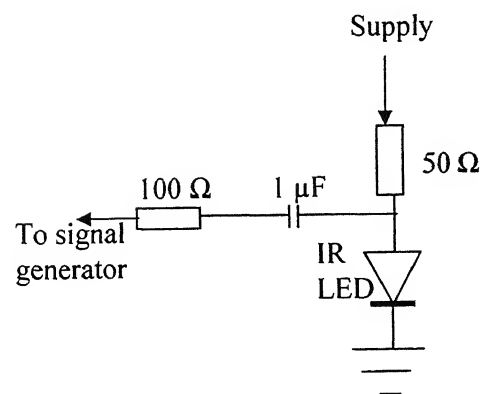
Fig.5.3 **Transmitter circuit**

5.2.2 Receiver side

The receiver side consists of the following stages. First and the important component is the PIN photodiode (C30808 (N-type silicon pin) photodiode) which

converts the incident light into equivalent current variations. The next stage is a transimpedance amplifier which converts the input current into an equivalent voltage. The output voltage is viewed on a high frequency digital storage oscilloscope (TDS1012, 100MHz, 1GS/s).

5.2.3 Interfacing part

The whole experiment is automated by connecting both the signal source and digital storage oscilloscope to a Pentium III PC through GPIB interface. A LabVIEW program is used for controlling the signal generator and oscilloscope through GPIB. The LabVIEW program, called VI, has all the features for synchronised operation of both transmitting and receiving part. The VIs used for the control of signal source and oscilloscope are shown in figs. 5.4 and 5.5, respectively. Fig. 5.6 shows the complete VI used for the measurement procedure.

Fig 5.4 **VI used for controlling signal generator**

Fig. 5.5 **VI used for controlling oscilloscope**
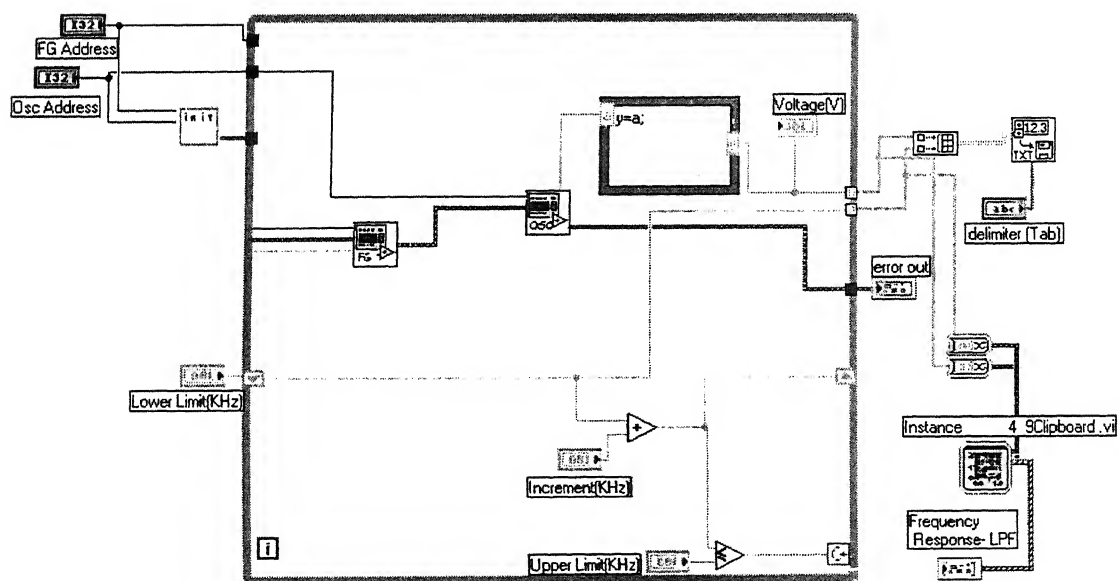
Fig. 5.6 **VI used for the automated measurement control**

5.3 MEASUREMENT PROCEDURE AND RESULTS

The signal source is adjusted continuously to emit sinusoidal signals of varying frequency in pre defined intervals. The output corresponding to each frequency input at the transmitter side is recorded at 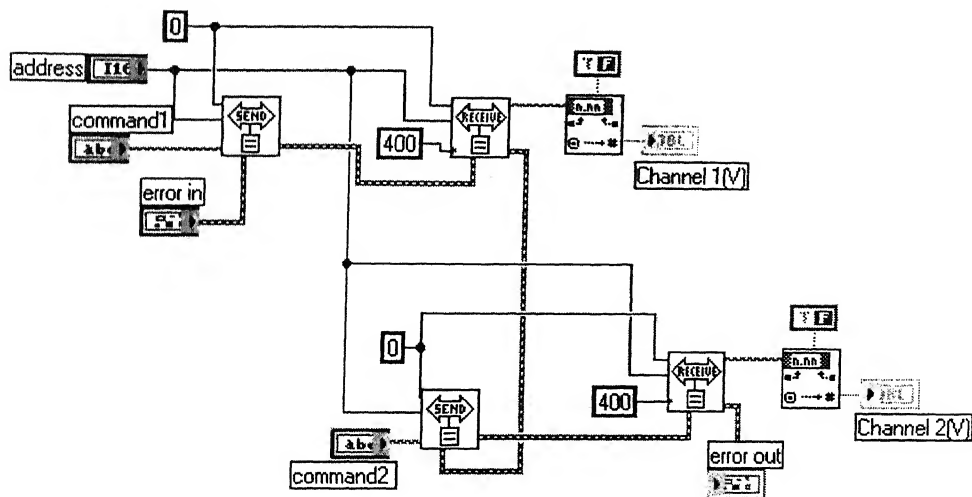the receiver side by an automated set up. Frequency response plots are obtained keeping the transmitter at one position and varying the receiver positions. The x,y,z co-ordinates of the transmitter and receiver position for different frequency response measurement trials are tabulated in table 5.1 The different positions are showed in fig. 5.7. Table 5.2 gives the important measurement set up parameters.

Transmitter
(Location unchanged)

Receiver	Receiver	Receiver
(Location 1)	**(Location 2)**	**(Location 3)**

Fig. 5.7 **Transmitter and Receiver locations for different measurement trials**

Transmitter Location	(25,25,0)
Receiver Location (1)	(25,25,15)
Receiver Location(2)	(30,30,15)
Receiver Location(3)	(40,40,15)

Table 5.1 **Position coordinates (in cm) for different trials**

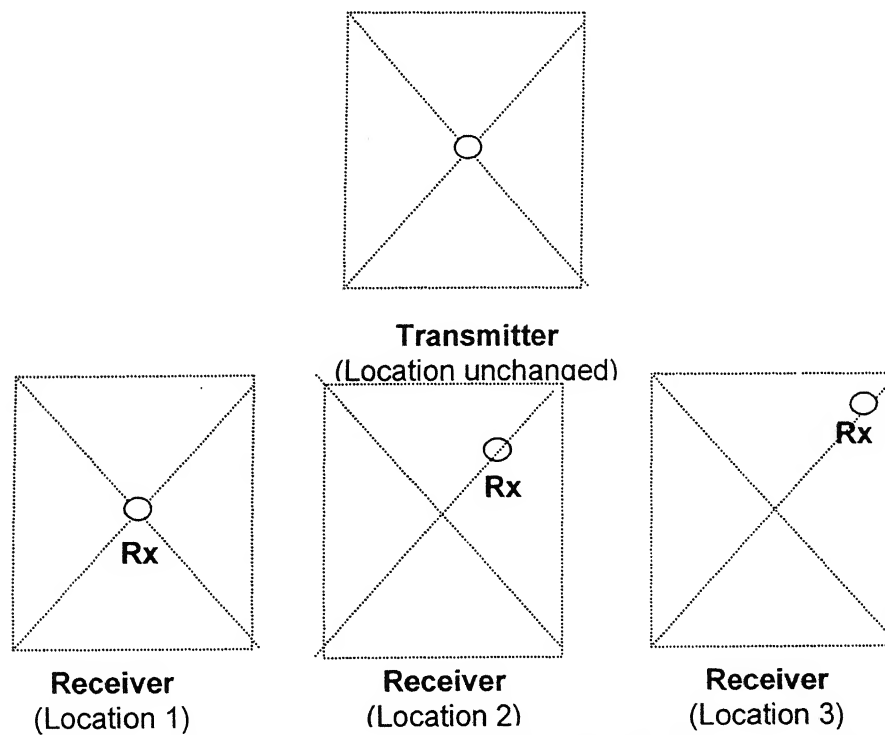| Operating wavelength	850 nm
Frequency Range of Measurement	100KHz- 2MHz
Average Optical output power of IR LED	2mW
Area of the photodiode	5mm² (Circular)
Responsivity of photodiode	0.65A/W

Table 5.2 **Measurement set up parameters**

Fig. 5.8 shows the magnitude response of the system for three different positions of the receiver, keeping transmitter at same positions.
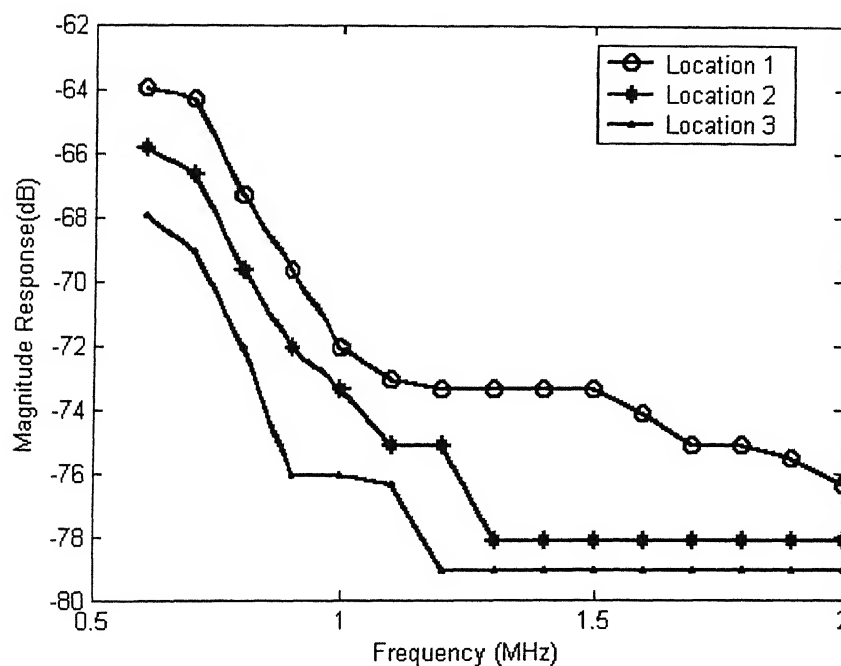
Fig. 5.8 **Frequency response plot of the system for 3 different receiver positions**

Fig. 5.8 shows the frequency response of the system for 3 different positions explained in table 5.1 and fig. 5.7. Observing the three plots, we note that it agrees with the conclusion reached in section 4.2 of chapter 4. The value of path loss is different at different locations of the receiver in the same room. The values of received power at same frequency in three different locations are different. Thus, this experiment also

supports the conclusion that path loss depends on the separation between transmitter and receiver. Location 1 is the nearest location to the transmitter. From fig.5.8, we see that the corresponding plot has the highest magnitude value of all the three for all frequencies. Location 3 is the farthest one from the transmitter. It has the lowest magnitude values. Thus the experiment also supports the statement that, path loss is very much dependent on the receiver and transmitter positions.

The values obtained are not accurate due to the frequency response limitations of the receiver circuit. We used TL-081 operational amplifier in the trans-impedance configuration. TL-081 has a gain-bandwidth product of 4 MHz. Hence the circuit response is poor at higher frequencies and did not give much information about system bandwidth. In order to get better estimates of the channel bandwidth the receiver must have bandwidths of at least 40MHz as can be seen from earlier works [15]-[19], [27] [28].

CHAPTER 6

CONCLUSIONS AND SUGGESTIONS FOR

FUTURE WORK

The aim of the thesis was to characterise the infrared diffuse channel using a suitable functional model. This thesis has presented a detailed study of the different propagation properties involved in the infrared wireless communication system using diffused IR light. The results of various studies can be summarised as follows:

- Diffuse multi path propagation results in pulse spreading of the signal which can be quantified using the rms delay spread parameter. The value of this spread varies significantly with change in the position of transmitter, receiver or both. The value depends upon the room dimensions, the separation between the transmitter - receiver and the separation from the ceiling.

- The second effect of multi path propagation is the path loss. This is also highly dependent on the position of the transmitter and receiver, their separation from the ceiling and the room size.

- Impulse response and hence the frequency response of a system is highly influenced by the room configuration and position of transmitter and receiver. The 3dB bandwidth, which defines the maximum data rate possible for a system, is hence different for different arrangements even in the same room. So while designing indoor diffuse communication systems, prime importance has to be given to the positioning of transmitter and receiver so that it caters to the need of maximum data rate required. In case of highly mobile systems, some compromise will have to be made, since the problem of variations in system bandwidth with position is unavoidable in the case of infrared diffuse channels.

- Bit error rate of diffused infrared system depends on various factors, viz. received power, data rate, background power level, filter bandwidth (if any used), and the delay spread due to dispersion.

- The power penalty due to dispersion is an important deciding factor on the data rate that can be used for a particular communication system. The value of maximum data rate obtained for a tolerable level of power penalty agrees very much with the 3dB bandwidth found in frequency response analysis.

- The final conclusion at which we arrive after a detailed characterisation of the infrared channel is that, the rms delay spread and channel path loss are highly correlated. Hence by knowing one of them, the other one can be easily found out. The estimation of rms delay spread found using this method may not be a highly accurate result, but is quite a good estimate in most circumstances.

6.1   SUGGESTIONS FOR FUTURE WORK

- Infrared indoor wireless communication is a topic which allows for a lot of research in its different aspects. This work concentrated only on a single functional model. Various other models have been developed so far. The variation of different parameters with configuration can be studied using different other impulse response models as well and their accuracy can be compared.

- This work assumes both transmitter and receiver to be pointing vertically to the ceiling. The other case, i.e., both pointing to the centre of the ceiling can be studied in detail.

- In this thesis, the only variation explored is the change of position. Two other studies may be explored - the effect of receiver rotation on channel path loss and rms delay spread, and the effect of receiver shadowing and blockage.

- The experimental studies used non-standard transmitter and receiver developed using discrete components. Hence accurate experimental results on channel frequency response could not be obtained. Standard transmitter and receiver modules having high bandwidth capabilities may be used to estimate the system bandwidth and the frequency response. Also the effect of receiver rotation and shadowing can be studied.

REFERENCES

[1].J.M. Kahn and J.R. Barry, "Wireless Infrared Communications," *Proc. IEEE*, vol. 85, pp. 265-298, Feb. 1997.

[2].D. Mavrakis: "Measurement and prediction of the wideband indoor radio and infrared channels," Ph.D. dissertation, University of Surrey, Oct 2002.

[3].A.C. Boucouvalas, Indoor Ambient light noise and its effect on wireless optical links," *IEE Proceedings: Optoelectronics*, vol. 143, pp 334-338, Dec 1996.

[4].A.J.C. Moreira, R.T. Valadas, and A.M. de Oliveira Duarte, "Performance of infrared transmission systems under ambient light interference," *IEE Proceedings: Optoelectronics*, vol. 143, pp 339-346, Dec 1996.

[5].Z. Ghassemloy, " Indoor Optical Wireless Communication Systems- Part I: Review," *http://soe.unn.ac.uk/ocr/downloads/partI-rev.pdf*, 2003

[6].D.J.T. Heatley, D.R. Wisely, I. Neild, and P. Cochrane," Optical wireless: the story so far," *IEEE Commun. Mag.*, vol. 36, pp. 72-82, Dec 1998.

[7].F.R.Gfeller and U.H. Bapst, "Wireless in-house data communication via diffuse infrared radiation," *Proc. IEEE*, vol. 67, pp. 1474-1486, Nov. 1979.

[8].J.R. Barry, J.M. Kahn, W.J. Krause, E.A. Lee, and D.G. Messerschmitt, "Simulation of multipath impulse response for wireless optical channels," *IEEE J. Select. Areas Commun.*, vol.11, no.3, pp. 367-379, Apr 1993.

[9].J.R. Barry, *Wireless Infrared Communications*. Boston: Kluwer Academic, 1994.

[10].J.B. Carruthers and J.M. Kahn, "Modeling of non-directed wireless infrared channels," *IEEE Trans. Commun.*, vol. 45, pp. 1260-1268, Oct 1997.

[11].R. Perez Jimenez , J. Berges, and M.J. Betancor, "Statistical model for the impulse response of infrared indoor diffuse channels," *Electron. Lett.*, vol. 33, no.15, pp. 1298-1300, 1997.

[12]. R. Perez Jimenez, V.M. Melian, and M.J. Betancor, "Analysis of multipath impulse response of diffuse and quasi-diffuse optical links for IR-WLAN," in *Proc.14th Conf. IEEE Comp. Commun. Soc.*, pp. 924-930, 1995.

[13]. F.J. Lopez Hernandez, R.Perez-Jimenez, and A. Santamaria, "Monte Carlo calculation of impulse response on diffuse IR wireless indoor channels", *Electron. Lett.*, vol.34, no.12, pp. 1260 –1261, 1998.

[14]. Carruthers, J.B., and Kannan, P.: 'Iterative site-based modeling for wireless infrared channels', *IEEE Trans. Antennas Propag..*, vol. 50, pp. 759–765, May 2002.

[15]. H. Hashemi, G. Yun, M. Kavehrad, F. Behbahani, and P. Galko, "Indoor propagation measurements at infrared frequencies for wireless local area networks applications,"*IEEE Trans. Veh. Technol.*, vol. 43, pp. 562-576, Aug 1994.

[16]. H. Hashemi, G. Yun, M. Kavehrad, and F. Behbahani, "Frequency response measurements of the wireless indoor channel at infrared frequencies," in *Proc. Int. Conf. Communications*(ICC'94), pp. 1511-1515, 1994.

[17]. J.M. Kahn, W.J. Krause, and J.B. Carruthers, "Experimental characterization of nondirected indoor infrared channels," *IEEE Trans. Commun.*, vol. 43, no. 2-4, pp. 1613-1623, Feb./Mar./Apr. 1995.

[18]. M. Pakravan, M. Kavehrad, and H. Hashemi, "Effects of rotation on the path loss and the delay spread in indoor infrared channel", *Proc. Int. Conf. Communications* (ICC'98), July 1998

[19]. M.R. Pakravan, Mohsen Kavehrad, and H. Hashemi, "Indoor infrared channel characterization by measurements," *IEEE. Trans. Veh. Technol.*, vol. 50, pp. 1053-1073, July 2001.

[20]. J.M. Kahn, J.R. Barry, M.D. Audeh, J.B. Carruthers, W.J. Krause, and G.W. Marsh,"Non-directed infrared links for high-capacity wireless LANs," *IEEE Personal Commun. Mag.*, vol. 1, no. 2, pp. 12-25, May 1994.

[21] C.R. Lomba, R.T. Valadas, and A.M. de Oliveira Duarte, "Experimental characterisation and modelling of the reflection of infrared signals on indoor surfaces," *IEE Proc. Optoelect.*, vol. 145, no.3, pp. 191-197, June 1998.

[22] H. Chan, K.L. Sterckx, J.M.H. Elmirghani, and R.A. Cryan, "Performance of optical wireless OOK and PPM systems under the constraints of ambient noise and multipath dispersion", *IEEE Commun. Mag.*, vol. 36, pp.83-87, Dec 1998.

[23] T.S. Chu and M.J. Gans, "High speed infrared local wireless communication," *IEEE Commun. Mag.*, vol. 25, pp. 4-10, Aug 1987.

[24] J.R. Barry, J.M. Kahn, E.A. Lee, and D.G. Messerschmitt, "High speed nondirective optical communication for wireless networks," *IEEE Netw. Mag.*, pp. 44-54, Nov. 1991.

[25] G.W. Marsh and J.M Kahn, "Performance evaluation of experimental 50-Mb/s diffuse infrared wireless link using on-off keying with decision-feedback equalization," *IEEE Trans. Commun.*, vol. 44, pp. 1496-1504, Nov. 1996.

[26] M.D. Audeh and J.M. Kahn, "Performance evaluation of baseband OOK for wireless indoor infrared LANs operating at 100Mb/s," *IEEE Trans. Commun.*, vol. 43, pp. 2085-2094, June 1995.

[27] K. Smitha and J.John, "Propagation measurements of indoor infrared channels," *Proc. Photonics-2004*, 2004.

[28] Q. Jiang, M. Kavehrad, M. Pakravan, and M. Tai, "Wideband optical propagation measurement system for characterization of indoor wireless infrared channel," *Proc. Int. Conf. Communications* (ICC'95), Seattle, WA, 1995, pp. 1173-1176, 1995.

APPENDIX A

The Simpson's 1/9 rule for calculating double integrals

The calculation of a double integral of the function f(x,y) in the rectangular domain

R ={a<x<b, c<y<d} in which the x-interval is divided into n parts while the y-interval is

divided into m parts (m and n even), can be accomplished by using

$$I = \frac{\Delta x . \Delta y}{9} \sum_{\substack{i=2 \\ i=i+2}}^{n} \sum_{\substack{j=2 \\ j=j+2}}^{m} S_{ij}$$

where

$$S_{ij} = f_{i-1,j-1} + f_{i-1,j+1} + f_{i+1,j-1} + f_{i+1,j+1} + 4\left(f_{i-1,j} + f_{i,j-1} + f_{i+1,j} + f_{i,j+1}\right)$$
$$+ 16 f_{ij}$$

The x-interval gets divided into n parts with $x_1 = a$, $x_2 = a + \Delta x$, $x_3 = a+2.\Delta x$, ..., $x_{n+1} = b = a+n.\Delta x$, so that

$$\Delta x = \frac{b-a}{n}$$

Similarly, the y-interval gets divided into m parts with $y_1 = b$, $y_2 = b+\Delta y$, $y_2 = b+2.\Delta y$, ...,

$Y_{n+1} = b+n.\Delta y$, so that

$$\Delta y = \frac{d-c}{m}$$

Any double integral can be found out by applying the above formula properly.